Progress in Oceanography 183 (2020) 102293

Contents lists available at ScienceDirect

Progress in Oceanography

journal homepage: www.elsevier.com/locate/pocean

Net community oxygen production derived from Seaglider deployments at the Porcupine Abyssal Plain site (PAP; northeast Atlantic) in 2012–13

U. Binetti[a,*], J. Kaiser[b], G.M. Damerell[b], A. Rumyantseva[c], A.P. Martin[d], S. Henson[d], K.J. Heywood[b]

[a] Centre for Environment, Fisheries and Aquaculture Science (Cefas), Cefas Laboratories, Pakefield Road, Lowestoft NR33 0HT, UK
[b] Centre for Ocean and Atmospheric Sciences, School of Environmental Sciences, University of East Anglia, Norwich, United Kingdom
[c] School of Ocean and Earth Sciences, University of Southampton, Southampton, UK
[d] National Oceanography Centre, Southampton, UK

ARTICLE INFO

Keywords:
Dissolved oxygen
Biological production
Algal bloom
Ocean-atmosphere system
North Atlantic
Porcupine Abyssal Plain
Gliders

ABSTRACT

As part of the OSMOSIS project, a fleet of gliders surveyed the Porcupine Abyssal Plain site (Northeast Atlantic) from September 2012 to September 2013. Salinity, temperature, dissolved oxygen concentration and chlorophyll fluorescence were measured in the top 1000 m of the water column. Net community production (*N*) over an annual cycle using an oxygen-budget approach was compared to variations of several parameters (wind speed, mixing layer depth relative to euphotic depth, temperature, density, net heat flux) showing that the main theories (Critical Depth Hypothesis, Critical Turbulence Hypothesis, Heat-flux Hypothesis) can explain the switch between net heterotrophy to net autotrophy in different times of the year, The dynamics leading to an increase in productivity were related to shifts in regimes, such as the possible differences in nutrient concentration. The oxygen concentration profiles used for this study constitute a unique dataset spanning the entire productive season resulting in a data series longer than in previous studies. Net autotrophy was found at the site with a net production of (6.4 ± 1.9) mol m^{-2} in oxygen equivalents (or (4.3 ± 1.3) mol m^{-2} in carbon equivalents). The period exhibiting a deep chlorophyll maximum between 10 m and 40 m of depth contributed (1.5 ± 0.5) mol m^{-2} in oxygen equivalent to the total *N*. These results are greater than most previously published estimates.

1. Introduction

Marine net biological production (*N*) is the balance between oxygen (O_2) production by phytoplankton during photosynthesis and O_2 consumption during respiration by the entire marine community. The seas around the world harbour almost half of the global plant production (Field et al, 1998; Williams, 1998), moving carbon and oxygen within and across compartments and reservoirs. By causing supersaturation or undersaturation of surface waters, biota is able to drive fluxes between the ocean and the atmosphere. This makes the ocean a carbon sink or a source depending on biological activity, which is important for estimating the global carbon budget and understanding how CO_2 influences climate as a greenhouse gas (Falkowksi, 1998).

Measurement of *N* over the entire annual cycle are important to understand the metabolic balance of the open ocean (i.e., the sign and magnitude of *N*), which is the focus of a long-running debate (del Giorgio et al., 1997; Duarte and Agustí,1998;Williams 1998; Williams and Bowers, 1999; del Giorgio and Duarte, 2002; Karl et al., 2003; Hansell et al., 2009; Ducklow and Doney, 2013; Williams et al., 2013; Duarte et al, 2013). Uncertainty about *N* derives from the use of different methods for the calculation of *N* and its components. Several biases are known to affect *in vitro* measurements and their comparability with the real ocean (Williams et al., 1998; Kaiser et al., 2005). There are also challenges in separating the influence of biological and physical processes on *in situ* measurements (Hamme and Emerson, 2006; Emerson et al., 2008). It is not even clear what some of the methods used are actually measuring (Regaudie-de-Gioux et al., 2014).

The analysis of *N* variations within the annual cycle, and their comparison with variations in other parameters, are instead useful to understand what factors are limiting or stimulating production and to investigate the validity of different mechanisms proposed so far. In regimes of nutrient limitation, gradual deepening of the mixed layer into nutrient-richer waters has been recognised as a plausible explanation for autumn blooms (Marra et al., 1990; Findlay et al., 2006). More recently, productivity peaks have been related to pulses of nutrients created by the interaction between wind and surface currents

* Corresponding author.
E-mail addresses: Umberto.binetti@cefas.co.uk, u.binetti@uea.ac.uk (U. Binetti).

https://doi.org/10.1016/j.pocean.2020.102293

Available online 07 February 2020

(Rumyantseva et al., 2015). The discussion about what triggers autotrophy when nutrients are not limited is more complicated. The Sverdrup Hypothesis (Critical Depth Hypothesis or CDH, Sverdrup, 1953) sees light as a driving factor: the plankton community is productive when the mixed layer is shallower than the critical depth, which is the depth above which total production exceeds total respiration. Since 1953, a long discussion has flourished to confirm or refute the Sverdrup CDH and new hypotheses have been proposed based on its weak points such as the assumption of phytoplankton behaving as a passive tracer. New hypotheses focus on the influence that turbulence has on the ability of the phytoplankton to access light. According to the Critical Turbulence Hypothesis (CTH, Huismann, 1999), high turbulence displaces the plankton at a faster rate than its growth rate. When turbulence decreases below a critical value, plankton grows faster than it is displaced and this leads to blooms (i.e., accumulation of oxygen and chlorophyll at the surface). Taylor and Ferrari (2011) linked the turbulence to the net heat flux, suggesting that the inversion from negative heat flux (water cooling) to positive heat flux (water warming) and the consequent shut down of convective mixing is a reliable parameter to predict the start of the bloom on an interannual timescale (Heat Flux Hypothesis or HFH). Enriquez and Taylor (2015) proposed another model linking the variations in turbulence induced by wind stress and water cooling (negative net heat flux leading to convective mixing) to the depth of the mixing layer. They predicted that when the mixing layer shoals, the phytoplankton respond with an increased growth rate (and then increased production). Behrenfeld (2010) suggested the Recoupling-Dilution Hypothesis, according to which phytoplankton has a positive growth rate when the mixed layer is deepening because of lower predation pressure.

The first goal of the present study is to estimate the magnitude of *N* in the productive layer of the water column through the analysis of variations of the oxygen inventory over time, based on oxygen concentration measured *in situ* by underwater gliders. Thanks to the high frequency of glider measurements and considering the length of this time series, the present study tries to overcome limitations in calculating *N* due to low spatial or temporal resolution. The present study surveyed an area located in the North Atlantic, in the proximity of the frequently sampled Porcupine Abyssal Plain (PAP) Sustained Observatory. This allows us to compare *N* estimates with results of previous studies that focused on the same area (e.g., Körtzinger et al., 2008a; Frigstad et al., 2015) along with basin-wide estimates. Furthermore, the availability of a suite of different parameters provided insights into the mechanisms that trigger increases in production. The second aim of the paper is to compare variations in N with other parameters to understand how observation fit with the different theories suggested to explain the increase in productivity.

2. Material and methods

2.1. Data acquisition

The OSMOSIS project included five cruises and three glider missions performed at PAP (Fig. 1) between September 2012 and September 2013. The cruises enabled the deployment and recovery of the gliders and the collection of a suite of *in situ* parameters to be used for calibration of the glider data. The three glider missions were carried out with short overlapping periods when the research vessels visited the area to swap gliders. Details of the glider campaigns, quality control, calibration and analysis of the physical oceanographic context of the year-long time series are provided by Damerell et al. (2016). During each mission two gliders operated at the same time moving along two separate butterfly- (or hourglass-) shaped transects oriented perpendicular to each other (one glider moving north-south and the other east-west) centred around 48.7°N and 16.2°W with 15 km long edges (Fig. 1). Because of a malfunctioning oxygen sensor and deviations from the designated transect, only one glider per mission was used to create

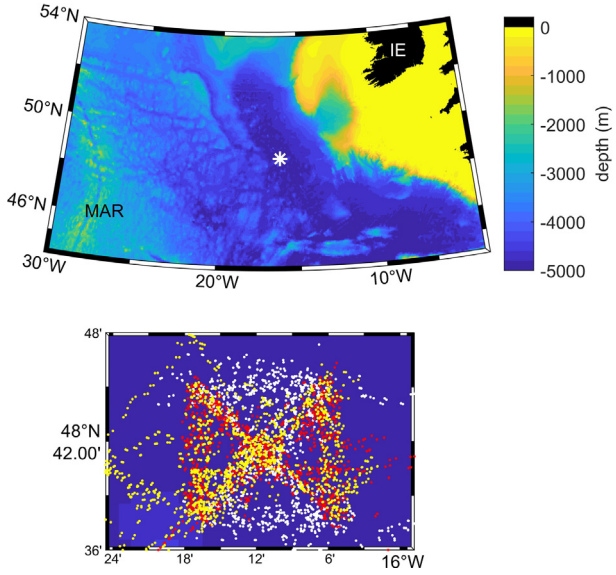

Fig. 1. Survey Location by the Porcupine Abyssal Plain Sustained Observatory. Top panel: survey location compared with ocean floor bathymetry. MAR is the Mid-Atlantic Ridge, IE is Ireland. Bottom panel: butterfly/hourglass paths described by gliders during the missios; point represent surfacing location of gliders: white is SG566 (first mission), red is SG502 and yellow is SG566 (second mission). (For interpretation of the references to colour in this figure legend, the reader is referred to the web version of this article.)

the year-long dataseries. Data from glider SG566 were considered between September 2012 and January 2013; SG502 between January 2013 and April 2013 and SG566 a second time between April 2013 and September 2013. The glider data are held at the British Oceanographic Data Centre and can be accessed at https://doi.org/10/cqc6.

2.2. CTD calibration

The calibration of the data followed several steps. Ship-CTD oxygen concentration, $c(O_2)$, profiles were calibrated against water samples analysed by Winkler titration. Glider $c(O_2)$ profiles were first adjusted to account for the response time of the optodes and subsequently calibrated against the Winkler-calibrated ship-CTD $c(O_2)$ profiles.

CTD casts were performed just before the deployment of the gliders and soon after their recovery. Oxygen concentration was measured by a Clark-type electrode (Seabird SBE43) attached to the rosette frame and water was sampled by the means of Niskin bottles attached to the same rosette. At the end of the cast, Winkler samples were collected from selected Niskin bottles and their $c(O_2)$ was measured by Winkler titration following WOCE protocols (Culberson 1991; Dickson,1996). For each cast, CTD $c(O_2)$ was calibrated by linear regression against Winkler-derived $c(O_2)$.

2.3. Response time correction

The gliders recorded $c(O_2)$ by means of optodes (Aanderaa Data Instruments; Tengberg et al., 2003), which measure the lifetime of the red light emitted by excited porphyrins in a sensing foil as a temperature-compensated phase difference (ϕ_{TC}), which depends on the $c(O_2)$. The diffusion time of the gas through the optode foil is characterised by a certain response time (τ). When plotting ϕ_{TC} against pressure, the response time shifts ϕ_{TC} profiles in the same direction the glider is moving in. Gradients will appear deeper than their actual depth when gliders descend and shallower when gliders ascend through the water column. A best-fit response time (τ) was determined from each pair of consecutive ascents and descents over the top 300 m. All response times of ascent-descent pairs in the same glider mission were fitted to a

normal distribution and its central value was used as τ to shift all the profiles of the same glider mission. The best-fit response times were applied to shift the profiles backwards in time, which resulted in a shift of the descent profiles upwards and the ascent profiles downwards. Variations and uncertainty in τ may be caused by variations in temperature and short-term changes in the vertical $c(O_2)$ profile during subsequent glider dives.

2.4. Glider calibration and despiking

The τ-corrected ϕ_{TC} profiles were calibrated using the Winkler-calibrated ship-CTD $c(O_2)$ profiles, using the closest CTD cast (< 4 km and < 3 h away). ϕ_{TC} profiles from several glider dives and several CTD profiles were used in the calibration as long as the glider and the ship were within the limits of proximity defined above.

Calibrated phase differences ϕ_{cal}(ship-CTD) were calculated from ship-CTD $c(O_2)$ as follows:

(1) calculate water vapour pressure p_{vap} using potential temperature and practical salinity;
(2) calculate oxygen saturation concentration $c_{sat}(O_2)$ using the parameterisation of Garcia and Gordon (1992) with the solubility coefficients of Benson and Krause (1984);
(3) calculate air saturation $s(O_2)$ equivalent to an atmospheric pressure of 1013.25 hPa where $s(O_2) = c(O_2)/c_{sat}(O_2)$;
(4) calculate partial pressure of oxygen, $\Delta p(O_2)$, using $s(O_2)$ and p_{vap}
(5) calculate ϕ_{cal} by inverting the manufacturer-provided sensing-foil specific polynomial that uses temperature, $\Delta p(O_2)$ and 21 coefficients (A_0 to A_{13} and B_0 to B_6) to derive ϕ_{cal}

ϕ_{cal}(ship-CTD) profiles and glider ϕ_{TC} profiles were then binned according to potential density and compared. The offset and slope of their linear regression was used as C_0 and C_1 in Eq. (1):

$$\phi_{cal}(\text{glider}) = C_0 + C_1\phi_{TC} \quad (1)$$

Since CTD casts were performed during the cruises at the deployment and recovery of the gliders, there was a linear calibration equation obtained at the beginning and at the end of each mission. In case the two calibration equations were not the same (indicating drift of the sensor over time), a time-varying C_0 and C_1 was calculated for each dive interpolating over time between the values at the beginning and end of each mission. Each dive had therefore a unique calibration equation that transformed ϕ_{TC} into ϕ_{cal}.

ϕ_{cal}(glider) profiles were then transformed into calibrated glider $c(O_2)$ with the same five steps used for the back-calculation of the CTD ϕ_{cal} in reverse order.

Spikes in the profiles were automatically flagged when a data point matched any of the following criteria:

(1) unrealistic $c(O_2)$, i.e values < 0 µmol kg^{-1} or > 1000 µmol kg^{-1};
(2) significant increase in the standard deviation of a $c(O_2)$ profile due to a single point;
(3) single points with anomalous $c(O_2)$ within water masses with constant concentrations;
(4) $c(O_2)$ values apparently above the surface (due to pressure sensor inaccuracies).

Visual despiking of profiles was carried out to remove anomalous $c(O_2)$ at the surface due to light hitting the foil, waves that expose the sensor to air or problems in τ correction.

At the end of the process, 527 points were flagged as spikes in SG566 (0.14% of the total), 837 in SG502 (0.22% of the total) and 546 in the second SG566 mission (0.14% of the total). All these spikes were in the upper 40 m of the water column. The uncertainty associated with the calibration of $c(O_2)$ values is expressed as the standard deviation of the residual difference between ship-CTD $c(O_2)$ and glider $c(O_2)$ after the calibration. The uncertainty for the whole dataset was computed as the mean of the uncertainties of the six different calibrations (one at the beginning and one at the end of each mission, 2.2 µmol kg^{-1}). With the uncertainty in the ship-CTD calibration against Winkler samples of 1.6 µmol kg^{-1}, the overall uncertainty associated with calibrating glider $c(O_2)$ was 2.7 µmol kg^{-1}.

At the end of the calibration, entire profiles were also flagged as anomalous and not considered in further calculations. In particular, the profiles recorded after the 11th August 2013 were disregarded because biofouling affected the optode of the SG566. Biofouling was identified by anomalous readings in $c(O_2)$ throughout the whole water column and its presence was confirmed by visual inspection when the glider was recovered. More details about biofouling during this survey are provided in Appendix A – Biofouling, including the explanation of why the 11th August was chosen as cut-off date.

2.5. Mixed layer calculation

The calculation of z_{mix} was performed for each of the 4035$c(O_2)$ profiles of the OSMOSIS time series using three consecutive glider missions (one glider per mission). $c(O_2)$ at 5 m depth (calculated by interpolation) was used as reference concentration, $c_{ref}(O_2)$, which is the estimate of $c(O_2)$ in the mixed layer. This depth is shallower than the one (10 m) chosen in previous studies (e.g. de Boyer Montégut et al., 2004, Castro-Morales and Kaiser, 2012), using the high-resolution data available all the way to the surface. Shallower depths were not considered because of noisiness of data in the very first metres of the water column. For 25 profiles the interpolation was not possible because their shallowest data-point was deeper than 5 m. For these profiles, the shallowest data-point of the profile was used as $c_{ref}(O_2)$. For 51 profiles the shallowest data point was deeper than 10 m; for these profiles $c_{ref}(O_2)$ and z_{mix} was not computed.

$c(O_2)$ profiles were smoothed by a local regression method using weighted linear least squares and a first degree polynomial model to eliminate possible effects of noise on the calculation. Forty random profiles with an obvious mixed layer were selected throughout the whole year and visually inspected to choose a threshold relative O_2 concentration change of 0.5%. This threshold is also in accordance with the one used for similar calculations by Castro-Morales and Kaiser (2012). Lower thresholds would result in random $z_{mix}(O_2)$ values not corresponding to a significant difference from $c_{ref}(O_2)$. The use of higher threshold would instead result in estimates of the mixed layer deeper than the actual layer visible in the profiles.

For each smoothed profile, the shallowest depth at which $|\Delta c|/c_{ref}$ (Eq. (3)) exceeded 0.005 was considered to be $z_{mix}(O_2)$

$$|\Delta c|/c_{ref} = |c(O_2)/c_{ref}(O_2) - 1| \quad (3)$$

2.6. Production calculation

Marine biological production (N) at the top of the water column was calculated analysing the changes in the oxygen inventory per unit area (I). Only the $c(O_2)$ profiles from glider descents were used for productivity calculations because some of the ascents were affected by spikes caused by sunlight hitting the optode foil near the surface (see Appendix A). The calculations focused on the top 60 m (z_{lim}) of the water column, which was equivalent to the mean euphotic depth (z_{eup}) of (60 ± 15) m during the study. z_{eup} was defined as the depth at which PAR falls to 1% of the level measured at the surface. PAR was measured *in situ* by sensor installed on the seagliders.

N was calculated as

$$N = \Delta I/\Delta t + F_{as} - E \quad (4)$$

where F_{as} is the air-sea O_2 flux (positive for O_2 outgassing), E is entrainment and N is net community production. ΔI was calculated as the $c(O_2)$ inventory change above z_{lim} between consecutive profiles. Profile

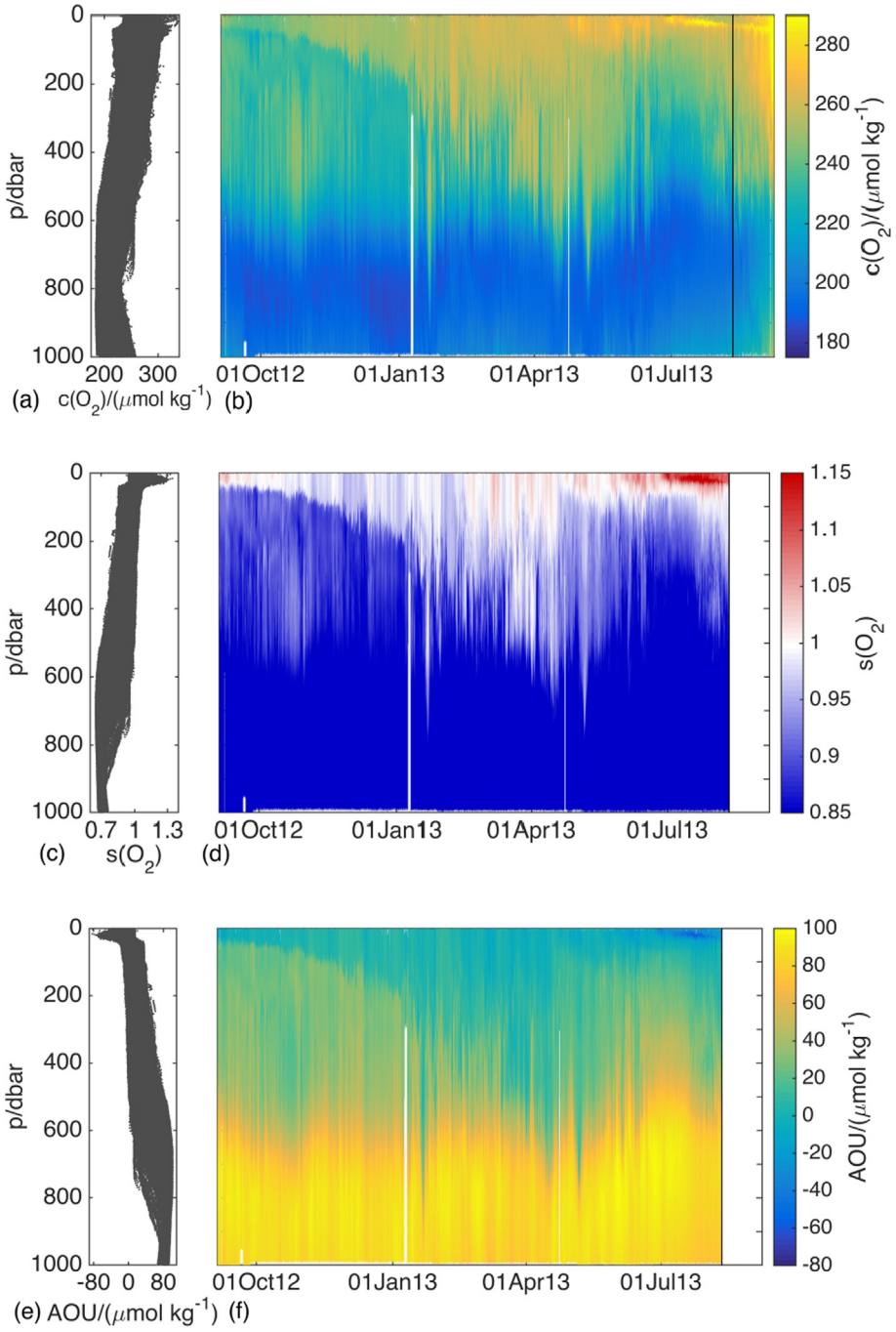

Fig. 2. Distribution against pressure (left panel) and time series against pressure (right panel) for (a and b) oxygen concentration, (c and d) oxygen saturation and (e and f) Apparent Oxygen Utilization. The black line in (b) marks the start of the biofouling.

inventory was calculated by integrating $c(O_2)$ over depth.

F_{as} was calculated using the correction for bubble injection (Δ) formulated by Woolf and Thorpe (1991):

$$F_{as} = k(O_2)[c(O_2) - (1 + \Delta)c_{sat}(O_2)] \quad (5)$$

where $k(O_2)$ is gas transfer velocity for oxygen; $c(O_2)$ is the dissolved oxygen concentration in the mixed layer; and $c_{sat}(O_2)$ is the oxygen saturation concentration calculated according to the Benson and Krause (1984) fit of Garcia and Gordon (1992) using the atmospheric pressure derived by interpolation of ERA-Interim reanalysis data (http://www.ecmwf.int/en/research/climate-reanalysis/era-interim, resolution of 6 h and 0.125° in latitude and longitude). $c(O_2)$ and $c_{sat}(O_2)$ used to calculate F_{as} were derived from the mean value for the top 10 m or as the mean above z_{mix} when $z_{mix} < 10$ m. The gas transfer velocity at a Schmidt number $Sc = 600$ was parameterised following Nightingale et al. (2000) using the daily averaged wind speed at 10 m derived from ERA-Interim reanalysis with the same resolution as the atmospheric pressure. F_{as} used to calculate N between two profiles was the mean of the F_{as} measured for these two profiles. It is worth noting that Song et al. (2015) compared ERA-Interim data with measurements from eight buoys, showing a good agreement between re-analysis and *in situ* measurements (regression coefficients for wind speed was above 0.7 and for direction was greater than 0.79). However, ERA-Interim over-estimated wind data at the buoy stations, with the max difference of 1.8 m/s; and 13% ERA-Interim wind data below 6 m/s were flagged as not good. There is therefore the possibility that F_{as} used here might be

slightly overestimated.

Entrainment was considered as the change of $c(O_2)$ due to deep water mixed all the way to the surface in the mixed layer when z_{mix} deepens. Entrainment could be positive or negative, corresponding to an increase or a decrease of the oxygen inventory. E between any two profiles at times t_1 and t_2 was considered only when z_{mix} deepened and when z_{mix} at t_2 was deeper than z_{lim}. Otherwise, E was equal to zero, e.g. when z_{mix} deepened, but remained above z_{lim}, a redistribution of the oxygen was assumed without any O_2 flux occurring through z_{lim} and therefore no variation in the oxygen inventory above z_{lim} ($I(z_{lim})$). In order to calculate z_{mix} deepening and shoaling, z_{mix} values were smoothed using a moving filter with 5 points span.

This was an Eulerian rather than Lagrangian study and therefore part of ΔI between adjacent profiles was the signal of geographical heterogeneity (patchiness) and horizontal advection. Advection has been considered negligible in previous studies (Emerson et al., 2008; Nicholson et al., 2008; Nicholson et al., 2015) due to the rapid effect of air-sea O_2 flux inequilibrating the concentration at the surface. However, Alkire et al. (2014) and Hull et al. (2016) showed that advection can significantly affect N estimates over time scales of days/months and for spatial scales less than 50 km. In this study, in order to consider the effect of advection, the individual N values measured between consecutive profiles were averaged over 7 days. Looking at the time-series, 7 days was in fact a period longer than the glider took to traverse the distance between large N values (sign of glider entering a O_2-rich advected water mass) and large negative N values (gliders getting out of the advected water mass). Averaging over 7 days was considered therefore an effective way to cancel out the positive and negative contribution of any water mass advected in the area to N calculation. This is also in line with Alkire et al. (2014), which in a similar glider experiment showed that the time scale of advection processes was around 4 days. In the present study, running averages of N for overlapping 7 day-long bins were assumed to be a valid estimate of biological activity (sensitivity to averaging period is tested in Appendix B).

The period of 7 days is also the approximate time any glider took to complete its butterfly- or hourglass-shaped transects and the averaging therefore gave estimates of N for the entire surveyed area, disregarding its internal geographical heterogeneity.

The variation in c(O2) were also analysed in relation to the thermal exchange between atmosphere and the ocean. In order to so this, the timeseries of net heat flux (H) was obtained from ERA-Interim reanalysis. The resolution of 6 h and 0.125° in latitude and longitude.

3. Results

3.1. Annual time series

The distribution of oxygen measured by the gliders at PAP between September 2012 and September 2013 is plotted against time and depth in Fig. 2, along with oxygen saturation ($s(O_2)$), ratio of $c(O_2)$ over $c_{sat}(O_2)$) and Apparent Oxygen Utilization (AOU, difference $c_{sat}(O_2)$ – c (O_2)). The other physical parameters measured concurrently with $c(O_2)$ are shown in Fig. 3. The vertical distributions suggest the presence of three layers in the water column. These layers have also been described by Damerell et al. (2016) who analysed salinity and temperature measured concurrently with the oxygen concentrations analysed in the present study. The top layer was roughly 150 m deep. This layer included the ocean surface boundary layer and had a seasonal cycle in the temperature due to solar insolation. Salinity was more variable, it did not follow any seasonal cycle and varied at all time scales, probably due to horizontal advection, local air-sea interaction and vertical mixing. The intermediate layer, between 150 m and 700 m, was characterised by a significant intra-seasonal variability in temperature and salinity, also strongly intercorrelated. This variability was mostly linked to gyre-scale and mesoscale dynamics rather than the surface forcing. Bottom layer was between 700 and 1000 m and had high variability at all timescales in temperature and salinity, strongly influenced by the Mediterranean Outflow Water (MOW) that appeared at these depths. This paper focuses on the top layer because the euphotic depth was always shallower than 100 m at any time and, therefore, the plankton blooms were restricted to in this layer.

In the top layer, $c(O_2)$ varied between 215 μmol kg^{-1} and 315 μmol kg^{-1} and $c_{sat}(O_2)$ between 224 μmol kg^{-1} and 273 μmol kg^{-1}. During winter $c(O_2)$ and $c_{sat}(O_2)$ both increased. $c(O_2)$ increased from mid-February onwards (Fig. 2b), with an alternation between periods of super- and undersaturation, which is reflected in the alternation of red and blue areas near the surface in Fig. 2d. At the beginning of July, $c(O_2)$ increased at the top 20 m of the water column, but c(O_2) quickly decreased at the very surface above 10 m of depth. At the same moment of this surface depletion, a deep chlorophyll and oxygen maximum developed between 20 m and 40 m of depth (Fig. 2b and Fig. 3h). High $s(O_2)$ (up to 1.18) and negative AOU (-44 μmol kg^{-1}) were measured in this shallow oxygen maximum (from 14th to 28th July between 10 m and 20 m). The $s(O_2)$ and c(Chl a) are correlated for c(Chl a) higher than 0.5 mg m^{-3}. In Fig. 4 it is possible to see a tendency to higher $s(O_2)$ when there was higher c(Chl a) (Fig. 4c and d). $s(O_2)$ for c(Chl a) lower than 0.5 mg m^{-3} were influenced by physical rather than biological processes because the algal biomass was too low to produce significant quantities of O_2. This was particularly obvious from September to March (Fig. 4). Data from July and August showed higher $s(O_2)$ with respect to March-June.

In order to calculate N, the physical factors affecting $c(O_2)$ variations (F_{as} and E) were calculated. F_{as} depends on the difference between $c(O_2)$ and $c_{sat}(O_2)$ following Eq. (5) (Fig. 5a). There was supersaturation ($c(O_2) > c_{sat}(O_2)$) in September at the beginning of the timeseries and after May. There was a period of undersaturation ($c(O_2) < c_{sat}(O_2)$) lasting from November until March and then a period of quasi equilibrium from March to May. F_{as} varied between -193 mmol m^{-2} d^{-1} and 155 mmol m^{-2} d^{-1}, with a mean value of (-13 ± 53) mmol m^{-2} d^{-1}. F_{as} showed a strong seasonality, with a short period of outgassing at the beginning of the timeseries, followed by a long period of ingassing from the end of September to the beginning of March (Fig. 5c). This was in turn followed by two months of quasi equilibrium with weaker influx and, from the end of May, F_{as} switched sign and started a period of outgassing that lasted until the end of the mission. Over nearly an annual cycle, this region of the North Atlantic is shown here to be a sink of oxygen rather than a source, with 4.8 mol m^{-2} of O_2 absorbed by the ocean during the surveyed period. This is driven by pulses of strong influx due to high wind that induce high bubble influx (Δ, Fig. 5b), but also by the late-occurring supersaturation. The data after 11th August 2013 were disregarded because of biofouling, making the time series one month shorter than an annual cycle (see Appendix A). This missing month was probably a productive period and therefore its inclusion would have likely increased the magnitude of the annual outgassing if taken into account.

The other element in the calculation of N was entrainment, E. When z_{mix} did not deepen below z_{lim}, E was considered to be zero (Fig. 6). When z_{mix} deepened, but remained above z_{lim}, it was assumed that a redistribution of the $I(z_{lim})$ occurred without any O_2 flux occurring through z_{lim}. Also, when z_{mix} shoaled, the change in $I(z_{lim})$ was assumed not to be related to any mixing with deeper water masses below z_{lim} and, therefore, no E was assumed to occur.

Fluctuation in z_{mix} linked to geographical variability and to the sensitivity of the threshold used for z_{mix} computation would affect E because deepening events are not compensated by the shoaling events in the calculation. In order to mitigate the effect of z_{mix} variability on N calculation, z_{mix} values were smoothed using a moving average filter over 5 datapoints (black line in Fig. 6a).

The values of N were calculated as the variation in $c(O_2)$ (ΔI) between consecutive profiles not explainable by F_{as} and E. Values were averaged over one week to disregard the effect of advection in the area. The time series of N averaged in overlapping bins of 7 days is plotted in

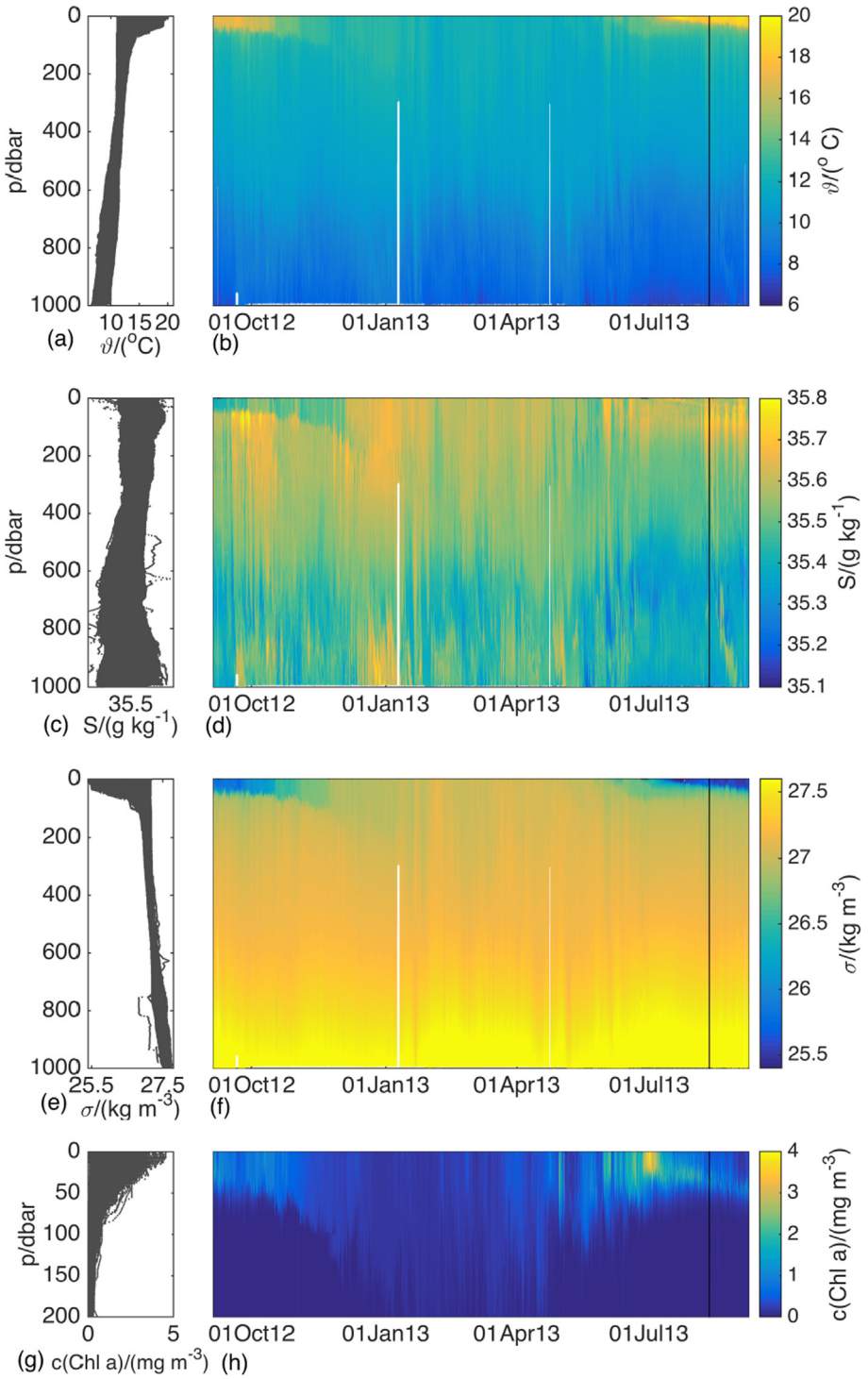

Fig. 3. Distribution against pressure (left panel) and time series against pressure (right panel) for (a and b) temperature, (c and d) salinity, (e and f) potential density at surface and (g and h) chlorophyll *a* concentration above 200 m. The black line in (b-d-f-h) marks the start of the biofouling.

Fig. 7 along with the averaged values of $\Delta I(z_{lim})/\Delta t$, F_{as} and E. The cumulative N between September 2012 and August 2013 is 6.4 mol m^{-2} and the mean N was 19 mmol m^{-2} d^{-1}. These values show net autotrophy in the area over an annual cycle.

Four periods (Table 1) where recognised within the cycle of N (Fig. 8). First period is the autumn season between 15th September and 20th November 2012. From 21st November, N dropped to negative values for several weeks, apart for some positive peaks. Towards the end of this mostly heterotrophic period, N started oscillating and from 10th February remained positive until the 3rd May. This long autotrophic period is here considered the start of the spring period. After other oscillations at the end of the spring period, another prolonged period of positive N starting from 20th June is considered as the start of the summer period, with the development of a deep chlorophyll maximum, DCM, and a shallow oxygen maximum.

3.2. Autumn bloom

During the autumn period, net autotrophy alternated with net heterotrophy (Fig. 9a). During the first switch from net respiration to net

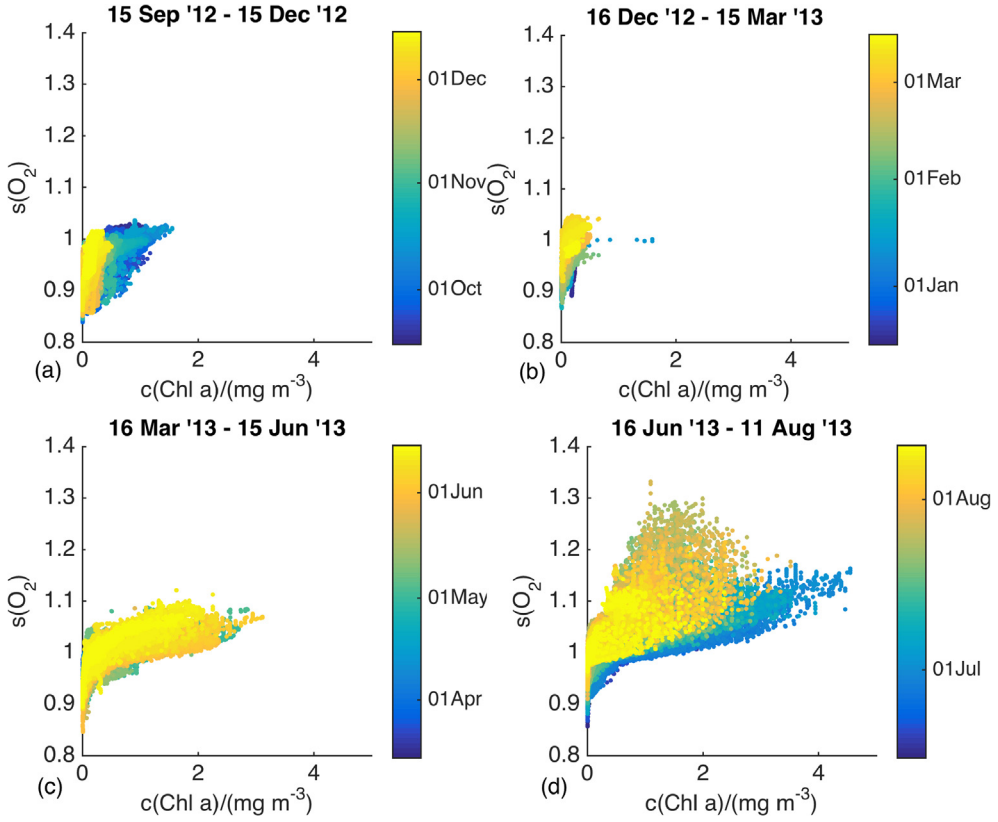

Fig. 4. Distribution of oxygen saturation against chlorophyll *a* concentration coloured by the date of measurements between mid-September 2012 and mid-December 2012 (a), mid-December 2012 and mid-March 2013 (b), mid-March 2013 and mid-Jund 2013 (c) and mid-June 2013 to mid-August 2013 (d).

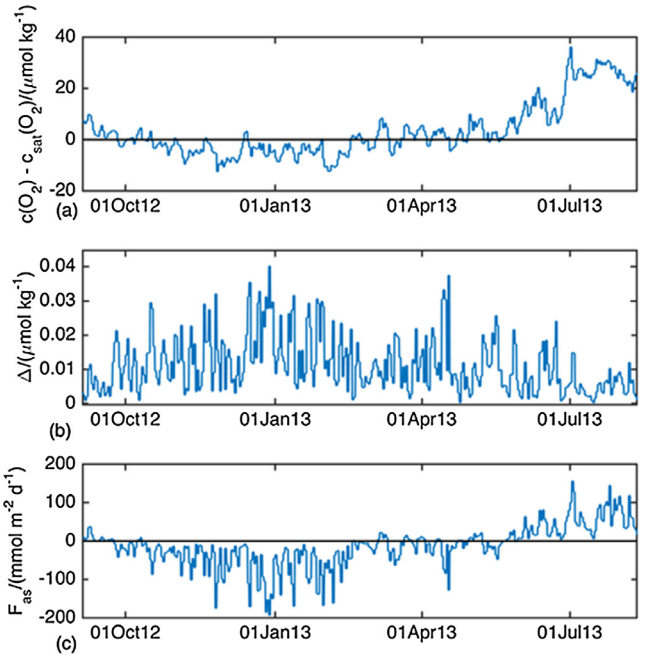

Fig. 5. (a) Difference between daily mean oxygen concentration and daily mean oxygen concentration at saturation in the top 10 m used in the air-sea oxygen flux calculation. Positive values indicate supersaturation and negative values indicate undersaturation; (b) bubbles supersaturation parameterisation (Δ) according to Woolf and Thorpe (1991); (c) air-sea oxygen flux. Positive values indicate outgassing of oxygen in the atmosphere and negative values indicate influx of oxygen in the water column.

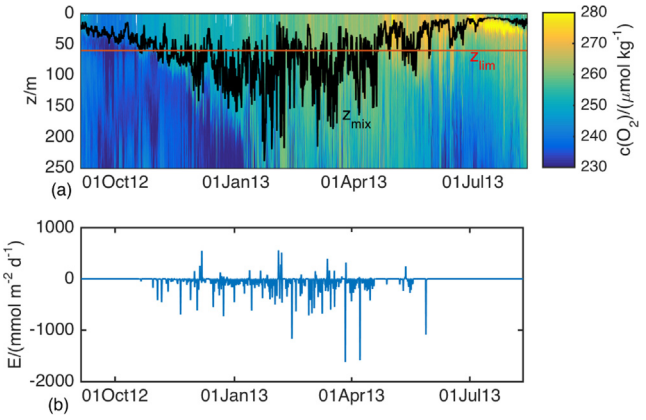

Fig. 6. (a) oxygen concentration versus depth with smoothed mixing layer depth (black line) and z_{lim} = 60 m (red line); (b) entrainment flux, i.e. rate of change of oxygen concentration due to entrainment. (For interpretation of the references to colour in this figure legend, the reader is referred to the web version of this article.)

production on the 27th September *N* reached a magnitude of (16 ± 12) mmol m^{-2} d^{-1} in oxygen equivalent. This peak in productivity lasted until 2nd October, and at the same time chlorophyll *a* concentration, *c*(Chl *a*), increased as well (Fig. 7d) as already discussed by Rumyantseva et al. (2015), They linked this peak to the passage of a storm that was in the area from the 24th to the 27th September 2012, as shown by the U_{10} values (Fig. 9c).

After 8th and 18th October, *N* and *c*(Chl *a*) increased again when the wind slowed down after sharp peaks (interpreted as storms). Between 30th October and 6th November, z_{mix} gradually deepened (black line in Fig. 9b) and *N* peaked again. However, when the wind

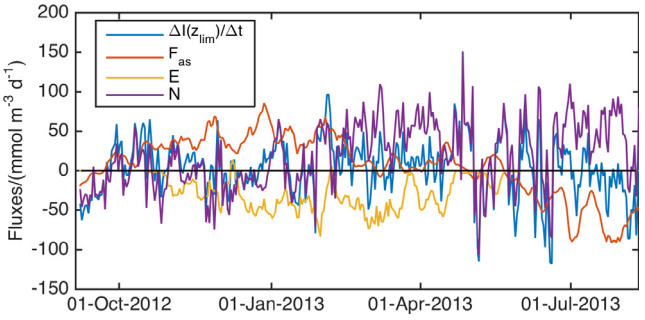

Fig. 7. Time series of oxygen fluxes: $\Delta I(z_{lim})/\Delta t$ in blue, F_{as} in red, E in yellow and N in purple, calculated as in Equation (4). All values are 7-day averages. Note that sign of air-sea O_2 flux is here inverted in order to represent its contribution to N. (For interpretation of the references to colour in this figure legend, the reader is referred to the web version of this article.)

Table 1
Periods showing different productive regimes identified in the annual cycle with start and end dates and length in days.

Period	Start and end date	Length
Autumn bloom	15th Sep 2012 – 20th Nov 2012	67 d
Heterotrophic period	21st Nov 2012 – 9th Feb 2013	81 d
Spring	10th Feb 2013 – 19th June 2013	130 d
Summer and DCM	19th Jun 2013 – 11th Aug 2013	54 d

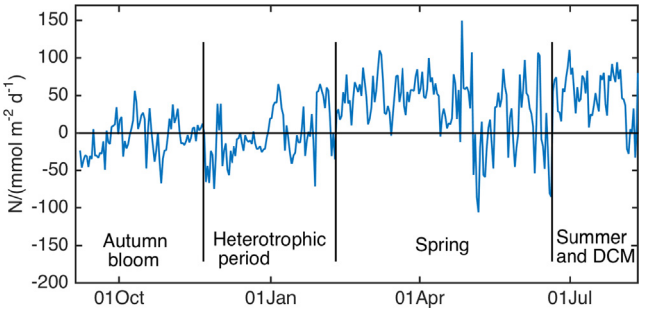

Fig. 8. Time series from September 2012 to August 2013 of net community production in oxygen equivalent divided in the four periods analysed separately.

slowed down and z_{mix} shoaled on the 6th November, N had negative values and c(Chl a) lowered, showing a decrease in productivity presumably due to a cut-off of nutrient supply from the deep. Afterwards, U_{10} increased and pushed z_{mix} deep again, possibly increasing the amount of nutrients in the water. However, z_{mix} did not stabilize again above z_{eup}, which could explain the absence of peaks in chlorophyll and the limited productivity.

Despite the production of 432 mmol m^{-2} (average (17 ± 14) mmol m^{-2} d^{-1}) during the authotrophic peaks, the community heterotrophy brings a net balance indistinguishable from 0 (11 ± 23) mmol m^{-2} d^{-1} between 26th September 2012 and 22nd November 2012.

3.3. Heterotrophic period

The period between 21st November 2012 and 9th February 2013 was characterised by a long initial period of heterotrophy (Fig. 10a; $N < 0$ for 62% of the time). Net consumption in the area was calculated at -0.3 mol m^{-2}.

Despite the mean N in this period was (-3 ± 34) mmol m^{-2} d^{-1}, the community seemed to go through a train of short peaks in production. These peaks (Fig. 11a) coincided with sharp changes in

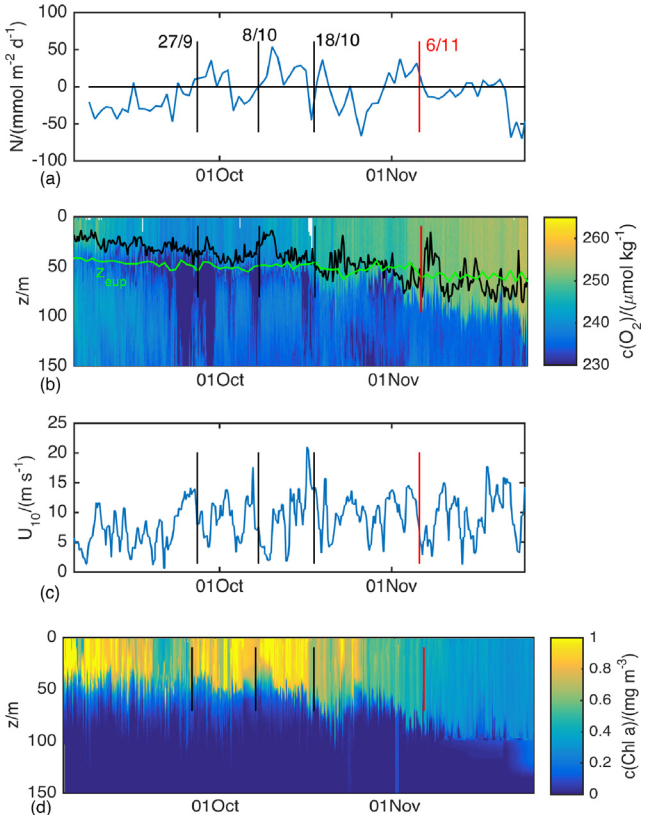

Fig. 9. (a) Running average of N over 7 days, (b) mixed layer and euphotic depths over oxygen concentration versus depth, (c) wind speed and (d) chlorophyll a concentration versus depth during the autumn bloom. Black vertical lines indicate the end of wind speed increases (storms) after which there was an increase in biological productivity. Red vertical line marks decrease in wind speed linked to the switch between net autotrophy and net heterotrophy during mixed layer depth shoaling. (For interpretation of the references to colour in this figure legend, the reader is referred to the web version of this article.)

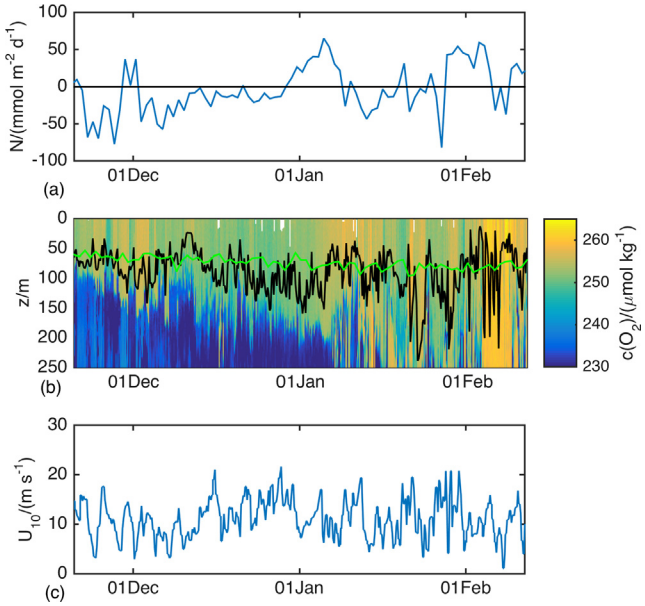

Fig. 10. (a) Net community production during the heterotrophic period; (b) oxygen concentration time series versus depth with z_{mix} (black line) and euphotic depth (green line); (c) wind speed at 10 m from sea surface from ERA-Interim reanalysis. (For interpretation of the references to colour in this figure legend, the reader is referred to the web version of this article.)

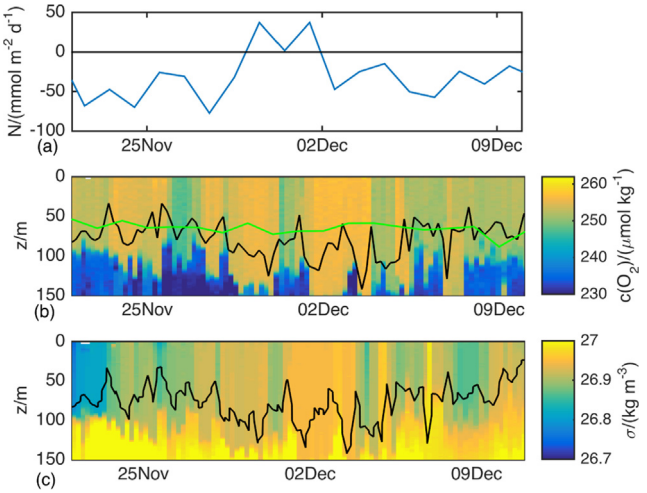

Fig. 11. (a) N, (b) oxygen concentration with euphotic depth in green and mixed layer in black and (c) potential density measured during the spike in N at the beginning of the heterotrophic period with mixed layer depth based on density. The obvious relation between variations in $c(O_2)$ and potential density (σ) suggests the presence of mesoscale features in the area. (For interpretation of the references to colour in this figure legend, the reader is referred to the web version of this article.)

potential density (visible in Fig. 11c), and this horizontal heterogeneity suggests that the glider was probably crossing a mesoscale feature, as discussed by Thompson et al. (2016). These are therefore likely false increases in *N*, since not related to biological activity. A valid correction for these values was not considered in this study and they were considered in the annual calculation of *N*. However, they represent an overestimation of biological *N*.

Between 30th December 2012 and 9th January 2013 there was a gradual transition towards a shallower $z_{mix,}$ which eventually became shallower than z_{eup} (Fig. 10b). This coincided with high *N* exceeding 65 mmol m^{-2} d^{-1}. In the same way, a decrease in wind speed and the shoaling of z_{mix} to the depth of z_{eup} coincided with the peak between 28th January and 6th February.

3.4. Spring

The spring season is here defined as the period between 10th February 2013 and 19th June 2013, 130 days during which the area was autotrophic ($N > 0$) with cumulative O_2 production of 4.5 mol m^{-2} and a mean *N* of (34 ± 44) mmol m^{-2} d^{-1} (Fig. 11). In this period, however, there was high variability (*N* standard deviation = 44 mmol m^{-2} d^{-1}) because production alternated with net respiration from the beginning of May (Fig. 13). Six 7-day bins of *N* estimates were above 100 mmol m^{-2} d^{-1} with a maximum of 149 mmol m^{-2} d^{-1}.

The period showed a series of *N* fluctuations. In February, despite minimal variations in *c*(Chl a), *N* is high. High levels of U_{10} are linked to periodic deepening of z_{mix}, that is however usually above z_{eup}, which indicate an increase in the amount of light experienced by the cells and, therefore, a boost in productivity. This also coincide with a period of H oscillating between negative and positive values, after a period of strong negative values. Another obvious feature is a short chlorophyll bloom happening in the upper 50 m of the water column between 24th and 28th February 2013, here called 'End-February Event' (EFE, Fig. 12a). This event happened when z_{mix} was very shallow (20–25 m), wind decreased and net heat flux (*H*, Fig. 12e) became temporarily positive (heat from the atmosphere to the ocean).

A larger peak in *N* occurred between 4th and 10th March when wind slowed down, *H* became temporarily positive again and z_{mix} shoaled with respect to z_{eup}. Another peak was visible between 16th

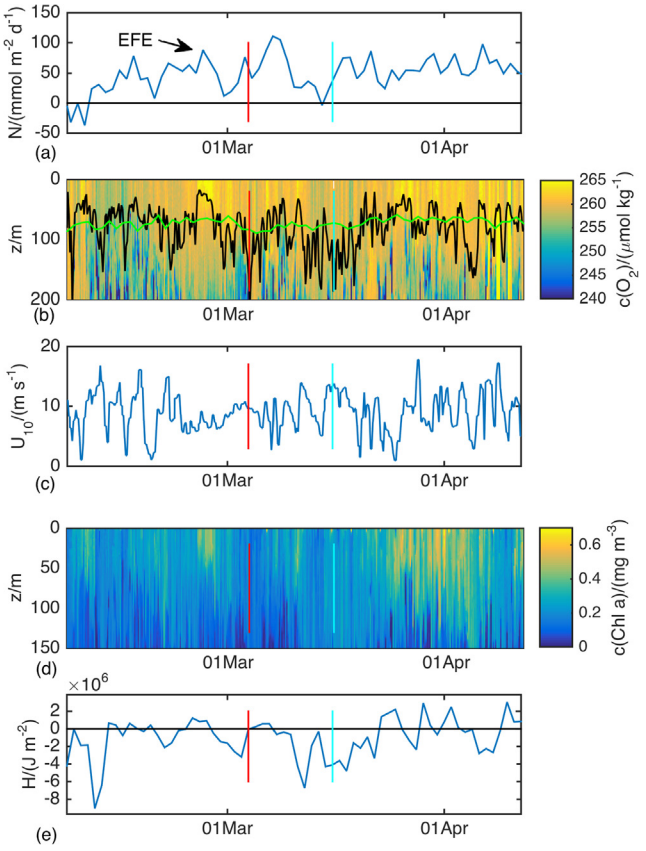

Fig. 12. (a) N, (b) mixed layer (black line) and euphotic depths (green line) over oxygen concentration versus depth, (c) wind speed, (d) chlorophyll *a* concentration versus depth and (e) net heat flux between (positive, heat from atmosphere to the ocean) 9th February and 12th April. Black vertical line indicates the start of the peak on 4th March and light blue line the start of the peak on 16th March. In panel (a) one can also see the peak associated with the end-February event (EFE). (For interpretation of the references to colour in this figure legend, the reader is referred to the web version of this article.)

March and 11th April 2013 when z_{mix} started to shoal again showing a reduction in mixing and, arguably, in turbulence. *H* was still negative, but it gradually increased towards a period of more stable positive values. During this peak z_{mix} varied significantly and *N* showed small decreases in its magnitude every time z_{mix} deepened and peaks every time z_{mix} shoaled near the surface.

The main spring bloom happened between 19th April and 27th May (Fig. 13), showing a substantial increase in *c*(Chl *a*). z_{mix} shoaled and stayed mostly stable above z_{eup}. This happened 10 days later than the switch of the heat flux from being mostly negative (water cooling) to mostly positive (water warming). However, *N* increased only when wind speed decreased on 19th April. The water retained at the surface became warmer and lighter, accumulating phytoplankton biomass. However, after 15 days (3rd May), *N* decreased suddenly, followed by a decrease in *c*(Chl *a*). Another interesting event starts on the 16th May, when wind speed increased and z_{mix} deepened. There was a slight increase of potential density and slight decrease of temperature showing that water from below the z_{eup}, probably enriched in nutrients, was mixed to the surface. Wind then decreased and *N* increased for a brief time, followed by an increase in $c(O_2)$ below z_{mix} rather than above, which could be evidence of low nutrient concentrations at the surface.

3.5. Summer bloom and deep chlorophyll maximum

From 20th June onwards, *N* was relatively high and above zero and z_{mix} was always shallower than z_{eup} (Fig. 14). This summer period as a

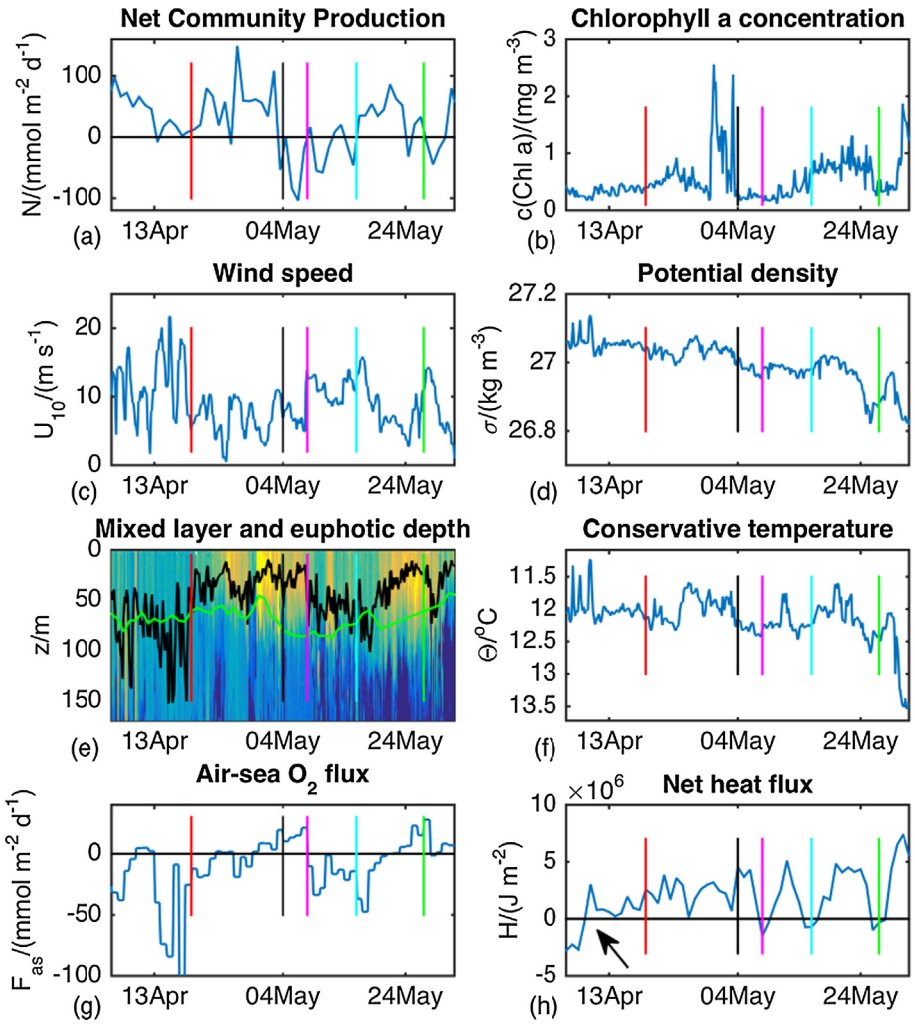

Fig. 13. Parameters associated with the N peak between April 19th and May 27th. (a) net community production above 60 m, (b) mean chlorophyll *a* concentration above 60 m, (c) wind speed (Era-Interim reanalysis), (d) mean potential density in the top 10 m, (e) mixed layer depth (in blue) and euphotic depth (in red) with background colours showing oxygen variations., (f) mean temperature in the top 10 m, (g) air-sea flux including bubbles and (h) net heat flux (ERA-Interim reanalysis). Red vertical line is the beginning of the peak (April 19th), black vertical line is the beginning of the heterotrophic period (May 4th), pink vertical line is the end of it (May 8th), light blue vertical line is the deepening event replenishing the nutrients above z_{mix} (May 16th) and green line is the end of the productive peak (May 27th). (For interpretation of the references to colour in this figure legend, the reader is referred to the web version of this article.)

whole had a mean *N* of (47 ± 36) mmol m^{-2} d^{-1} and produced 2.5 mol m^{-2}. The main features in this period are a surface bloom between 26th June and 4thJuly and the development of a deep chlorophyll maximum (DCM). The surface bloom was very productive with a mean *N* of (71 ± 24) mmol m^{-2} d^{-1}, reaching 110 mmol m^{-2} d^{-1}. However, since it lasted only 8 days, it produced only 0.6 mol m^{-2}. There was also an increase in *c*(Chl *a*). The bloom ended when wind increased again and z_{mix} deepened.

From 8th July wind decreased (Fig. 14c) and the water column transitioned to a regime of low turbulence and strong stratification. A DCM developed and the production increased significantly. Both the subsurface oxygen- and chlorophyll-rich feature were above the z_{eup} of 60 m. During the time in which there was a DCM, the system remained productive until 4th August, when the productivity decreased along with an increase in wind speed, potentially leading to increased turbulence in the water. z_{mix} deepened within the DCM, eroding it and mixing it with surface waters. The decrease of N at the end of the DCM period occurred at the same time as a decrease in the *c*(Chl *a*). During the presence of DCM (30 days, 8th July to 8th August) 1.5 mol m^{-2} were produced with a mean *N* of (48 ± 32) mmol m^{-2} d^{-1}.

4. Discussion

4.1. Annual cycle of N

This study calculated the productivity of the plankton community at the Porcupine Abyssal Plain for an annual cycle based on variations in *c* (O_2). Data were acquired between surface and 1000 m depth, but the analysis focused on the production in the euphotic layer, which was always within the upper ~100 m of the water column. In winter, colder temperatures increased $c_{sat}(O_2)$ and triggered an influx of O_2 from the atmosphere that, considering the absence of substantial biological activity and the rapid gas exchange due to strong winds, was expected to equilibrate to saturation (Broecker and Peng, 1992; Woolf and Thorpe, 1991; Chester, 2000; Ito et al., 2004). However, the water stayed undersaturated during this period showing that the air-sea O_2 flux was not sufficient to saturate the water. These results confirm previous observations (e.g. Körtzinger et al., 2001; Russell and Dickson, 2003; Körtzinger et al., 2004; Keeling et al., 2010; Duteil et al., 2013) and model output (Ito et al., 2004), which also reported undersaturation in surface waters in several oceans.

Supersaturation was expected in the upper ocean during phytoplankton blooms, when biological production peaks. Biological processes increased $c(O_2)$ from mid-February onwards, but supersaturation was not persistent. The level of $c_{sat}(O_2)$ suggests that, instead of a continuous bloom, a series of minor blooms occurred from February onwards before the major spring bloom that started at the end of May, when *c*(Chl *a*) increased significantly. Assuming that air-sea flux works towards saturating water over time, then oxygen production by phytoplankton in an already saturated water mass should result in supersaturation ($s(O_2) > 0$). However, considering that the air-sea flux was not sufficient to equilibrate $s(O_2)$, it can also be argued that increases in $c(O_2)$ due to biological production might not always be enough for $s(O_2) > 0$. For this reason, the analysis of the production should not be

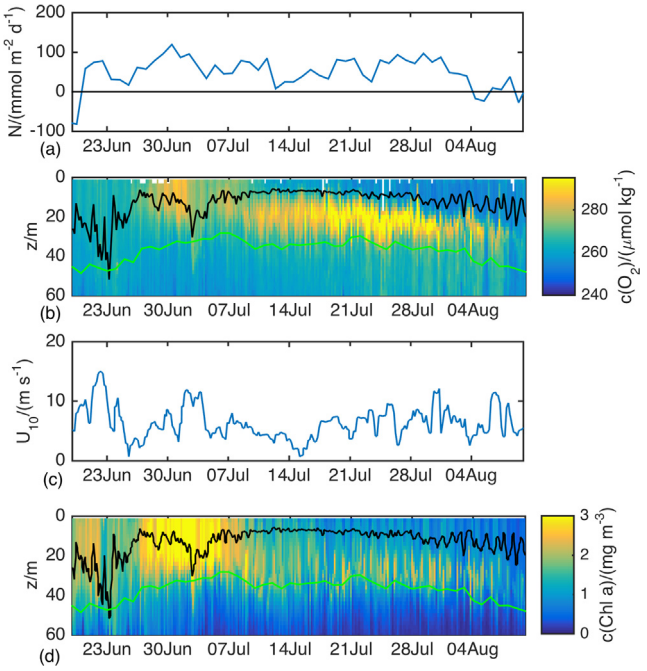

Fig. 14. (a) Net community production during the summer bloom and the deep chlorophyll maximum; (b) oxygen concentration over depth and time above zlim with zmix (black line) and zeup (green line); (c) wind speed at 10 m above sea-surface from ERA-Interim reanalysis; (d) chlorophyll *a* concentration versus depth. (For interpretation of the references to colour in this figure legend, the reader is referred to the web version of this article.)

based only on the supersaturation pattern and potential increases of *c* (Chl *a*) in periods of undersaturation should be investigate analysing variations in oxygen budget.

At the end of the main bloom (beginning of July), $c(O_2)$ decreased at the surface, while a deep chlorophyll and oxygen maximum developed between 10 m and 20 m from 14th to 28th July. The level of $s(O_2)$ in relation to *c*(Chl *a*) seems to change between spring and summer, when $s(O_2)$ reaches the highest value of 1.18. This different relation could be related to a change in the phytoplankton community between spring and summer: the community of the deep chlorophyll maximum seems able more efficient, being able to produce more O_2 and supersaturate the water at lower *c*(Chl *a*) with respect to earlier periods of the year. Changes in the phytoplankton community, such as the succession of dominant species over time, are linked to variation in parameters in the water column; the decrease of silicates after the uptake during diatom blooms, is one of the phenomena that can drive these successions (Egge and Aksnes, 1992; Martin-Jézéquel et al., 2000) making diatoms bloom before autotrophic dinoflagellates (Margalef, 1978; Leterme et al., 2005; McQuatters-Gollop et al., 2007, Barton et al., 2013). Furthermore, dimensional classes within the same group show a succession related to the ability of smaller species to uptake nutrients more efficiently in oligotrophic environments (Barton et al., 2013). This might also be related to the cyclic changes in nitrate concentration shown in the area by Hartman et al. (2010). The changes in the length of day light has also been linked to changes in bacterioplankton composition, which in turn has been linked to changes in phytoplankton (Gilbert et al., 2012). Considering that each taxon produces a different amount of oxygen per mole of chlorophyll *a*, a change in the dominant taxa when productivity is moved in the deep chlorophyll maximum could explain the higher amount of oxygen per unit chlorophyll. It must also be considered that the same species have variations in its amount of chlorophyll *a*, for example because of photoacclimation (Sakshaug et al. 1997; Goericke and Montoya 1998; Henriksen et al. 2002), which means that variations in the amount of chlorophyll *a* per cell do not change linearly with the amount of O_2 produced. This shift in species and/or in the physiology of the cells is influenced by many environmental factors such as light intensity, nutrient availability or the regime of turbulence (e.g., Huisman et al., 2004; Veldhuis et Kraay, 2004; Brunet et al., 2008; Dimier et al., 2009, Barton et al., 2013). Considering that the formation of the summer deep chlorophyll maximum suggests a substantial attenuation of mixing forces and that the end of the main bloom can be related to low nutrients, it is reasonable to induce that environmental changes drove a shift in the phytoplankton community, which led to higher saturation per unit chlorophyll in the DCM. It shall be also considered that the reduced turbulence might have given time to phytoplankton to adapt to different levels of light and that photosensitivity might therefore have played a game in reducing productivity at the top of the water column.

The productive period (spring and summer together) spanned from 9th February to the start of biofouling on 11th August and had a time-integrated oxygen production of (7.1 ± 2.1) mol m^{-2} with a mean *N*

Table 2
Net community production in carbon equivalent, N_C (adapted and expanded from Alkire et al. 2014). In bold are the results from studies analysing N_C directly, while in normal characters are the estimates in oxygen unit converted to N_C using the photosynthetic quotient, PQ. In these cases the PQ value used for the conversion is indicated.

Study	Year	Period	N_C mmol m^{-2} d^{-1}	PQ used	Notes
This study	2013	Autumn Bloom	11	1.5	PAP station, top
		Spring	22		60 m
		19 Apr – 3 May	54		
		Summer	31		
		26 Jun – 4 Jul	46		
		DCM	32		
		Spring + Summer	26		
		Whole year	13		
Bender et al., 1992	**1989**	**13 days between Apr and May**	**52**		**JGOFS, North Atlantic 47N/20W**
Körtzinger et al., 2008a	**2004**	**May –Aug**	**25**		**PAP station**
Körtzinger et al., 2008b	**2005**	**mid May -Jul**	**50–70**		**Labrador Sea**
Alkire et al. 2012	2008	Apr	66	1.5	Early Bloom
		May	115		Main Bloom
		(average)	(90)		Iceland Basin
Alkire et al. 2014	2008	Apr-Jun	25	1.5	Considering Alkire et al. 2012
		3–26 Jun	43		+postbloom
					Iceland Basin
Ostle et al., 2015	2012	Apr – Sep	16	0.8	Basin-wide, region 2 (see Ostle et al., 2015)
Frigstad et al., 2015	**2003–2012**	**Feb – July 25**	**(72–6)**		**PAP site, Mixed Layer**

of (39 ± 41) mmol m^{-2} d^{-1}. The seasonal production was converted to C equivalents using the photosynthetic quotient (PQ) of 1.5 as in Alkire et al., (2014) and resultant N_C values are listed in Table 2.

Considering only the productive period, our study region produced N_C = (4.8 ± 1.4) mol m^{-2}. This value is lower than the (6.4 ± 1.1) mol m^{-2} estimated by Körtzinger et al. (2008a) but fits well with the (4.6 ± 0.9) mol m^{-2} estimated by Frigstad et al. (2015) for the PAP area over a similar time span. N_C is higher than the 3.0 mol m^{-2} estimated by Ostle et al. (2015) on a basin scale and the 2.1 mol m^{-2} estimated by Alkire et al. (2014) in a more northerly area (59°N instead of 49°N). The results therefore suggest that the region of the PAP site is particularly productive. In these comparisons it must be considered that previous studies focused on shorter productive periods, leaving unresolved the question on whether the ocean over one year is either a heterotrophic or an autotrophic system. The current results show autotrophy over the entire annual cycle in the productive top layer despite long period of heterotrophy (see Section 4.3). This result fits with previous works that show net production when incubation-free methods are used (Letscher and Moore, 2017) and support the position that this part of the ocean has positive net production. Despite the major focus of discussion about the trophic state of the ocean has been focused mostly on subtropical oligotrophic gyres (e.g., Williams et al., 2013; Duarte et al, 2013), our results should be taken in account in global budgeting to estimate the carbon cycle and to consider whether the ocean is a net sink or source of carbon.

Considering the whole time series, the PAP site was autotrophic between September 2012 and August 2013, with annually integrated net community O_2 production of (6.4 ± 1.9) mol m^{-2} a^{-1} ((4.3 ± 1.3) mol m^{-2} in C equivalents). This value was computed without the last month of the year, which was disregarded due to biofouling on the optode. However, the shape of the biofouled profiles showed a DCM above 60 m (data not shown). Biofouling and its progressive growth also show a productive phytoplankton community. The disregarded period can therefore be considered productive and the cumulative N of 6.4 mol m^{-2} is likely an underestimation of the real production in the area over the full year.

The annual production values are higher than previous annual N_C estimates of Quay et al. (2012) who estimated 2.8 mol m^{-2} in the subpolar North Atlantic Ocean or by Neuer et al. (2007) who estimated Nc = 3.3 mol m^{-2} as a mean between 1996 and 2000 in a more southerly area. The annual production estimated in the present study is instead similar to the 5.5 mol m^{-2} estimated by Ostle et al. (2015) for 2012 in their region 2 (where PAP site is located). This area was found in their study to be the most productive sector in the basin. This similarity, however, hide seasonal differences since estimates from Ostle et al. (2015) are lower during the productive period and higher during the winter.

The differences among studies are probably due to factors such as interannual variability in the area and differences in methods used for the calculations. N in the present study was an estimate of the production in the euphotic layer and, therefore, studies analysing variation at greater depths than z_{eup} are expected to be lower because of the respiration occurring deeper. For example, some of the studies compared here (e.g., Frigstad et al., 2015; Ostle et al., 2015) analyse the changes above z_{mix} rather than above z_{eup}, while others (i.e. Körtzinger et al., 2008a) use deeper z_{lim} (230 m) for the calculation of $I(O_2)$. The temporal patchiness of productivity also increases the variability among N estimates, especially when values are averaged over subsamples in the same productive period (Alkire et al., 2012).

4.2. Bloom initiation dynamics

Measuring N based on oxygen variations (direct by-product of photosynthesis) shows that heterotrophy and autotrophy alternate throughout the whole year. Different processes seem to trigger autotrophic peaks at different times of year. During autumn (nutrient limitation), N peaks have been related to pulses of nutrients created by the interaction between wind and surface currents (see Rumyantseva et al., 2015). However, the trigger for later N peaks seems to follow instead the gradual deepening of the mixed layer into nutrient-richer waters, a dynamic already suggested in previous papers (Marra et al., 1990; Findlay et al., 2006). This process also explains how peaks of N can develop at the end of the spring, when nutrient can be depleted as well after a big bloom.

When nutrient limitation could be excluded, N increased only when the mixed layer was shoaling while there was net heterotrophy during the winter, when the mixed layer was deepening. Our results therefore disagree with the Recoupling-Dilution Hypothesis. Instead, the present study presents evidence supporting the validity of the mechanism proposed by Enriquez and Taylor (2015). When nutrients are not limiting, the peaks in N are associated with decreasing wind speed and positive net heat flux, which in turn are linked to a shoaling mixing layer. Our results imply that the plankton community needs low turbulence conditions in order to bloom. The magnitude of the blooms also seems to be related to the relative depth of the mixing layer to the euphotic depth, rather than the critical depth used in Enriquez and Taylor (2015). The main blooms developed when z_{mix} shoaled near or just above z_{eup}. The increase of production when the mixing layer shoaled did not always correspond to significant increases of chlorophyll a concentration at the surface (Rumyanteva et al., 2019) but rather subsurface (e.g., the peak starting on 3rd March).

Most of the peaks of N are associated with positive net surface heat flux i.e. ocean warming. In particular, the start of the main bloom during spring coincided with the switch between a period of mean negative net heat flux and a period of mean positive net heat flux at the beginning of April consistent with the HFH theory of Taylor and Ferrari (2011). This suggests that the time of this switch in the sign of net surface heat flux could be used as a proxy to analyse interannual variability in the starting time of the main bloom. However, N increased after a delay due to the presence of a storm, showing the need to take into consideration the turbulence induced by the wind stress in order to have more accurate bloom timing estimates, as hypothesised by Chiswell (2011) and Brody et al. (2013).

This study also highlights the presence of peaks in productivity when chlorophyll concentration showed no variations, which have to be considered along with the chlorophyll fluorescence-defined blooms in order to analyse correctly the triggering factors that increase production. It is also important to use high temporal resolution *in situ* data instead of climatologies to better appreciate the high variability of the system. The use of the mixing layer depth instead of the mixed layer depth is important to analyse variations in turbulence that affect the plankton and its metabolic activity.

4.3. Autumn period

The presence of increased productivity during the autumn is well known for this part of the ocean and is usually referred as the “autumn bloom” (Colebrook, 1982; Longhurst et al., 1995; Dandonneau et al., 2004; Lévy et al., 2005; Neuer et al., 2007; Martinez et al., 2011). The term ‘bloom’ however suggests a prolonged period of stable productivity, which was not observed in this data series. In the present study in fact, a series of autotrophic peaks happened in this season at the end of storms. Production enhancement after storms has already been seen in previous studies (Babin et al., 2004; Son et al., 2006; Wu et al., 2008, Rumyantseva et al., 2015). This supports the notion that autumn blooms are sustained by nutrient pulses through the pycnocline due to shear spiking (Rippeth et al., 2005, Rippeth et al., 2009; Williams et al., 2013, Rumyantseva et al., 2015) generated by rapid change in wind stress (Pollard, 1980). This suggests that pulses of nutrients from below stimulate biological production in shallow and nutrient depleted mixed layers. In these post-storm blooms, wind has to decrease before N could peak.

In contrast, the last peak of this season (30th October to 6th November) was linked to the gradual deepening of z_{mix} and the introduction to the surface layer of nutrients from below. The decrease of c(Chl *a*) at the end of this productivity peak (Fig. 3d) marks the passage to a less productive regime, with N not increasing even when z_{mix} shoaled. This peak seemed therefore to follow the dynamics described by Marra et al. (1990) and Findlay et al. (2006) according to which the nutrient input fuelling the autumn bloom is caused by the gradual deepening of z_{mix}. These two different dynamics of N peaks were discussed by Dutkiewicz et al. (2001), who showed that increasing wind speed can enhance N by bringing nutrients towards the surface as well as decrease N moving phytoplankton cells deeper, where they consume more than they produce (for example during storms).

The peaks of productivity during autumn were of lower magnitude than in spring and the total N was not significantly different from 0. This is in line with the conclusions of Martinez et al. (2011) who showed an asymmetry in the magnitude of the blooms in different seasons. According to Martinez et al. (2011), there was a shift from the 1980s, when autumn blooms had a magnitude comparable with the spring blooms, to the present day, when autumn blooms are smaller than spring blooms, as we find here. Martinez et al. (2011) linked this change to the delayed deepening of z_{mix} at the end of the summer that now happens later in the year than in the past.

Lateral advection, presence of mesoscale events, change in zooplankton community or even the effect of wind and storms are other possible causes for the smaller magnitude of autumn blooms proposed by Martinez et al. (2011). The present study supports the conclusions of Martinez et al. (2011) of non-symmetric blooms between seasons, and uses *in situ* measurements to support their hypothesis, which was based on satellite data.

4.4. Heterotrophic period

Heterotrophic periods have been already recorded in the North Atlantic (see literature in Duarte et al., 2013), however their magnitude and impact on the annual metabolic balance are debated (Duarte et al., 2013). Multiannual studies show the inter-annual variability in the metabolic state of the ocean at this time of the year (November-February). Ostle et al. (2015) used basin-scale observations of $c(O_2)$ at the surface to measure N and found autotrophy throughout 2012 and low N (not statistically different from zero) in 2013.

In this study, pulses of positive N during the heterotrophic period were linked to the glider crossing a mesoscale feature. The averaging process was probably not able to fully eliminate the signal of this geographical heterogeneity in N because the feature stayed in the area longer than one week.

The feature crossed by the glider at the end of November – beginning of December 2013 (Fig. 11) had higher $c(O_2)$ and part of this might be actually due to production. However, the density of the water was lower and an increase in $c(O_2)$ was explainable by the solubility effect (higher $c_{sat}(O_2)$). This peak was therefore probably overestimating N.

Other peaks occurred when z_{mix} stopped deepening and shoaled above z_{eup}. The potential reduction in turbulence in these cases seems to be linked to higher productivity since the N peaks were interrupted when the wind speed increased again.

The consumption estimated in the heterotrophic period (0.3 mol m^{-2}) was one order of magnitude lower than the production estimates in the rest of the year. The present study therefore shows that the presence of potentially protracted periods of net heterotrophy in this part of the North Atlantic have only a moderate impact on the production on an annual scale.

4.5. Spring

The PAP site is located in the North Atlantic between the subpolar and subtropical gyres, where, according to Longhurst (1998), blooms are expected in May. The timing of this bloom and its intensity have high interannual and geographical variability (Ueyama and Monger, 2005; Henson et al., 2006; Henson et al., 2009; Kahru et al., 2011; Zhai et al., 2013; Cole et al., 2015) and this explains why, despite being one of the most studied systems in oceanography, the dynamics of the North Atlantic spring bloom have not been fully understood as yet.

The pattern of several parameters (wind speed, z_{mix} in relation to z_{eup}, temperature, density, net heat flux) was compared with variations of N, with several peaks in productivity observed before the main bloom between April and May. Following this comparison, possible explanations for the variations of production over time were suggested: the water near-surface was considered nutrient repleted at the beginning of spring, while nutrient-limitation was assumed to happen later on in the season, considering the seasonal pattern showed by Hartman et al. (2010) in this area. Variations in nutrients availability to phytoplankton could therefore be the cause of the oscillations between $N > 0$ and $N < 0$ in the second part of the spring, with phytoplankton becoming more productive when nutrients were supplied. However, the absence of direct measurements of nutrient concentrations in this study makes it difficult to confirm these speculations and extrapolate them to infer more general dynamics. At the end of this period there were rapid transitions between accumulation of oxygen at the surface and below z_{mix}. These were probably related to geographical patchiness and demonstrate the heterogeneity of biological production at this time of the year.

4.6. Summer and deep chlorophyll maximum

Changes in nutrient concentrations may have caused the variations of N seen during the summer. Particularly interesting in this period is the DCM that lasted for over 30 days in the area thanks to a well-stratified water column with a very shallow z_{mix} above 10 m. The presence of this feature suggests nutrient limitation in the upper water column, as shown in previous studies (Klausmeier and Litchman, 2001; Klausmeier et al., 2007, Denaro et al., 2013). When the DCM was present, N integrated stayed high, accounting for 38% of the cumulative N estimated throughout the whole study. The formation of the DCM is usually related to increases in biomass (Beckmann and Hense, 2007) and/or to adaptation in the chlorophyll content of the cells (Fennel and Boss, 2003). This feature is a challenge for N calculations based on remote measurements or on the sampling of the plankton community for *in vitro* incubation. The ocean colour measured by satellite-borne sensors can be biased if the DCM is shallower than ~45 m depth study (Stramska and Stramski, 2005), as found in the present, *de facto* decoupling fluorescence readings from the real value at the surface. Annual N estimates obtained with the method used here should therefore be of higher accuracy and reliability than the ones based on remotely sensed ocean colour.

The demise of the DCM is probably related to nutrient limitation. N decreased when z_{mix} started to deepen at the end of July; however, z_{mix} was still above z_{eup} and so the reduced productivity was not related to the limitation of light. Instead, wind speed increased and the ensuing vertical turbulence may have exposed the plankton to the nutrient depleted water above, lowering the production. Evidence of this is the decrease of c(Chl *a*) happening at the same time between 20 and 40 m. An alternative explanation could be the reduction of the photosynthetic performances in the cells due to changes in photosensitivity. The low turbulence could in fact narrow the difference between phytoplankton adaptation time and water mixing time, resulting in changes in the pigment physiology of the cells (Claustre et al., 1994).

From the end of June, F_{as} was coupled to N values. The entrainment in this period was negligible, thanks to the strong stratification that allowed the formation of the DCM. This F_{as} can then be considered biologically induced, as found by Kaiser et al. (2005) for systems with negligible vertical and horizontal mixing.

5. Conclusions

Net community production (N) above the mean euphotic depth near the PAP site from September 2012 to August 2013 has been calculated by analysing the variations in depth integrated oxygen concentration over time. The area is autotrophic, with a mean N value of 19 mmol m^{-2} d^{-1} and a total production of 6.5 mol m^{-2} and an estimated annual production of 7 mol m^{-2}. The analysis of the annual cycle of net community production shows the presence of four periods with different regimes: the autumn period, a heterotrophic period and two productive periods (spring and summer) separated by the depletion of nutrients after the spring bloom. During the summer a very productive deep chlorophyll maximum developed which was responsible for a significant portion of the annual production. The values calculated fit the range of published estimates of net community production in the North Atlantic basin and in the same area. The variations within this range are attributed in part to the differences among the methods used for the calculations and also to interannual variability.

Variations in production are associated with factors such as wind speed, net heat flux and mixing layer depth. The theories proposed in the last decades for the explanation of the blooms (Critical Depth Hypothesis, Critical Turbulence Hypothesis, Heat-flux Hypothesis) are consistent with each other in explaining different mechanisms for how the system passes from net heterotrophy to net autotrophy when favourable conditions are matched.

Declaration of Competing Interest

The authors declare no conflict of interest.

Acknowledgements

This work would not have been possible without the piloting skills of several colleagues at the University of East Anglia, National Oceanography Centre (Southampton) and California Institute of Technology, plus the contribution of many people not represented in the author list. The deployment and recovery operations of gliders has also been possible thanks to the scientists, technicians, officers and crews of the RRS Discovery (cruise D381), RV Celtic Explorer (cruise CE13001), and RRS James Cook (cruises JC085, JC087 and JC090). The study is part of the project OSMOSIS, funded by NERC grants NE/I020083/1 and NE/I019905/1 and supported by NSF award OCE 1155676. UB was supported by Cefas funding during the writing of this paper. GMD and KJH were supported during the writing of this paper by the European Research Council under the European Union's Horizon 2020 research and innovation programme (grant agreement n° 741120).

Appendix A. Biofouling

Fig. 1a shows that $c(O_2)$ increased throughout the water column in the last month of the time series. At the surface, $c(O_2)$ reached values that were higher than in the rest of the year, and also showed increases at depths where it had been stable for the rest of the year. A careful analysis of this period was therefore carried out in order to understand the reason for this phenomenon.

The presence of high $c(O_2)$ values near the surface was considered first. There was an anomalous increase in $c(O_2)$ that was particularly visible near the deep chlorophyll maximum, where $c(O_2)$ reaches 343 μmol kg^{-1} (Fig. 1). At the same time there was a discrepancy between the data

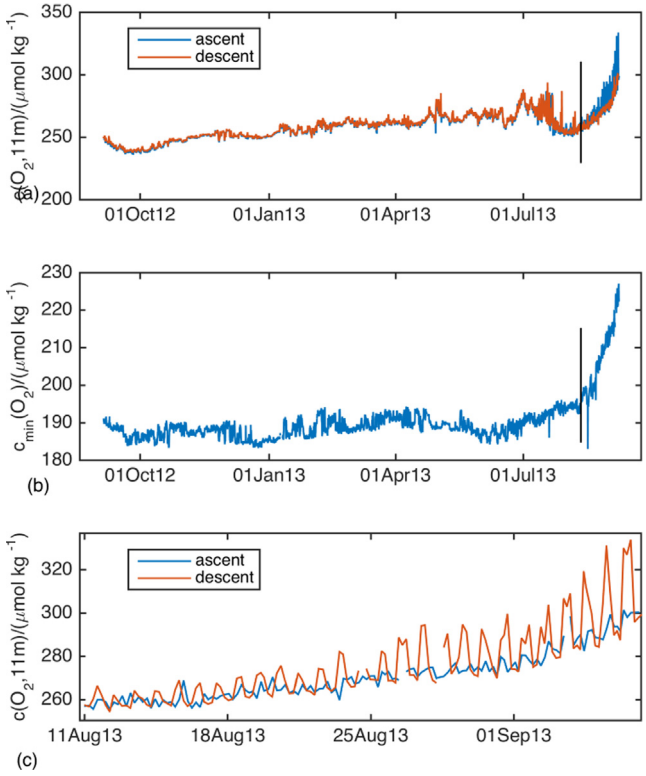

Fig. A1. (a) Oxygen concentration at the 11 m horizon during the ascending phase (blue) and descending (red) phase of glider dives; (b) Minimum oxygen concentration (if measured within the boundaries of Intermediate Water). In both (a) and (b) the black vertical line marks the date of August 11th, when the bias due to biofouling starts formally. (c) Focus from panel (a) during the biofouling-affected period showing the difference between ascents and descents that mismatched during daytime and matched again at night. (For interpretation of the references to colour in this figure legend, the reader is referred to the web version of this article.)

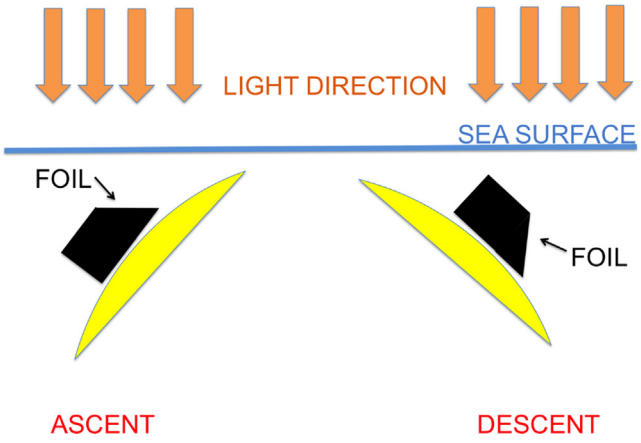

Fig. A2. Scheme of the position of the foil of the optode with respect to the surface and to the incident light in the ascents and descents of each dive.

collected during the ascent and the descent of each glider dive. Fig. A1 shows the concentration at 11 m as measured during descents and ascents. After 11th August, $c(O_2$,11 m) in the ascents is higher than in the descents. The magnitude of this difference increased over time, especially in the first metres of the water column down to the deep chlorophyll maximum (data not shown). However, during the night $c(O_2)$ values measured during the ascents and descents matched again (Fig. A1c).

Sunlight seems therefore to be a possible factor causing this difference. This was possibly related to the different angle that the optode had with respect to the incident light according to the direction of the glider (Fig. A2). The foil was virtually parallel to the surface in the ascents and more angled with respect to the incident light during the descents. This means that the probe was hit directly by the light when the glider went towards the surface, whereas it received less light when it went towards the deep. This was not enough to explain why the two phases of the dives are different in the last month of measurements, because otherwise this phenomenon would have been visible throughout the whole time series. There must have been therefore a new factor that, interacting with the foil and with the light, caused the difference between ascents and descents in this part of the year. The increasing mismatch between phases (Fig. A1 a-c) also showed that this new factor had a growing influence on the sensor over time.

In the last month of the dataset there was also an increase in $c(O_2)$ in the otherwise overall stable minimum $c(O_2)$, $c_{min}(O_2)$ (Fig. 14b). Being distant from the surface and from the euphotic depth z_{eup}, this deep water mass was expected to be stable because it was not exposed to the big perturbations due to air-sea exchange and biological productivity. After 11th August there was a fast and un-interrupted increase of $c_{min}(O_2)$ that reached 226 μmol kg^{-1}. Considering that this sharp increase in $c(O_2)$ at depth began at the same time as the discrepancy between ascents and descents (on 11th August), these events were considered to be caused by the same factor. The descents seem to be less affected, while ascents show obviously unrealistic values during the day (Fig. A1a). However, descents still show an increasing pattern over time, showing that data cannot be used despite the direction of the glider movement.

Biofouling of the foil was the most likely factor behind the phenomena just described. It probably developed on top of the optode foil after the beginning of the productive period, when chlorophyll *a* concentration at the top of the water column was higher than in the rest of the year (beginning of July 2013, Fig. 2h). This is usually a proxy for the presence of high phytoplankton biomass, which makes it plausible that phytoplankton started to grow into a biofilm on the foil. The algae, producing more O_2 when exposed to direct and stronger light (during ascents), would have caused the difference between profiles in different phases. O_2 produced by the biofilm would have given high $c(O_2)$ readings not reflecting the actual $c(O_2)$ in the water column. Furthermore, the amount of gas released by the biofilm would have been proportional to its biomass – the growth of the biofilm would explain why there was an increase in the difference between phases, of $c(O_2$, surface) and of $c_{min}(O_2)$. At the recovery of the glider, all the sensors were covered by a green biofilm (Stephen Woodward, personal communication). The data collected after 11th August are therefore considered not valid for the scope of this study. As a lesson learnt, datasets should be checked, especially when missions last for several months in productive areas; discrepancies between ascents and descents appearing during the day and disappearing during the night, and the increase of values in deep water masses that are usually stable should be signs to look for to spot the possible presence of biofouling and question the validity of the data.

Biofouling is a well-known problem in oceanographic measurements (Tosteson et al., 1982; Manov et al., 2004; Delauney et al., 2010). It has been advocated in previous studies to be the cause of drift in optical sensors mounted on both moorings (e.g., Kinkade et al., 2001; Manov et al., 2004; Heupel et al., 2008) and gliders (e.g., Nicholson et al., 2008; Cetinić et al., 2009; Krahmann et al., 2011). The interest of the scientific community for the new solutions that can reduce the biofouling (e.g., Manov et al., 2004; Whelan and Regan, 2006; Delauney et al., 2010; Lobe, 2015) is a clear evidence of the importance of this problem for oceanographic observations. The research is particularly active in the glider-users community since the biofouling can also affect the flight performances of these vehicles (Krahmann et al., 2011; Moline and Went, 2011). Possible options include installation of wipers for mechanical removal of the fouling and special foul releasing coating to reduce biofouling settlement and growth; however, hydrodynamic must be taken into account not to impact performances (Lobe, 2015).

Appendix B. Method sensitivity

In order to test the sensitivity of the method and determine the uncertainties associated with the *N* estimates discussed above, we assessed the influence of different parameters and choices made.

If glider ascents are used in the calculations, the mean *N* is 2% greater than calculated with descents (Fig. A3). However, considering that the optode was influenced in a different way during ascents and descents, this calculation could have been potentially influenced by the initial growth of biofouling at the end of the dataseries.

Since the mean and standard deviation of z_{eup} were 60 m and 15 m respectively, mean and total cumulative *N* were recalculated using 45 m and

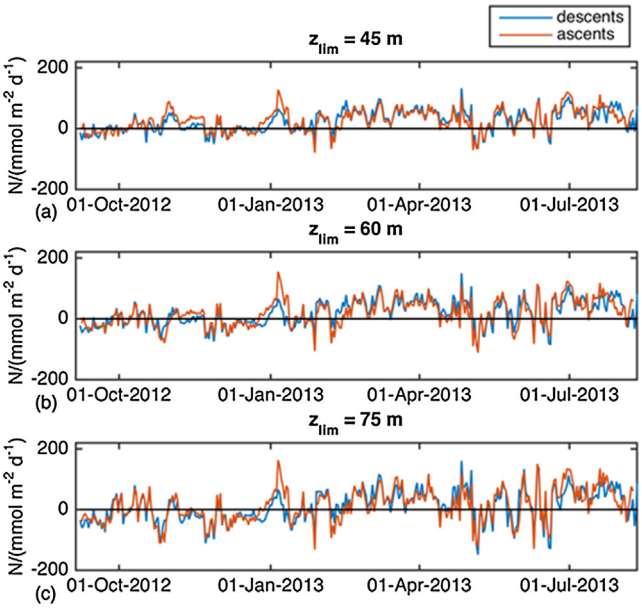

Fig. A3. Net community production time series measured above (a) 45 m, (b) 60 m and (c) 75 m using descents (blue lines) and ascents (red lines) from each glider dive. (For interpretation of the references to colour in this figure legend, the reader is referred to the web version of this article.)

Table A1
Net community production mean, standard deviation and total sum calculated above 45 m, 60 m and 75 m.

z_{lim} / m	Mean N / mmol m^{-2} d^{-1}	Standard deviation N / mmol m^{-2} d^{-1}	Total N / mol m^{-2}
45	24.7	35.1	8.4
60	19.0	43.0	6.5
75	12.1	52.7	4.1

Table A2
Mean values of the net community production time series obtained by averaging individual estimates between consecutive profiles over different bin lengths.

Mean N (mmol m^{-2} d^{-1} in O_2 equivalents) for time series obtained averaging over…							
1 day	3 days	5 days	7 days	9 days	11 days	13 days	15 days
19.0	18.9	18.9	19.0	19.2	19.6	20.0	20.3

75 m as z_{lim} (Table A1). These shallower and deeper z_{lim} were considered respectively an underestimation and overestimation of N in the euphotic zone. The shallower z_{lim} measure in fact only the very productive top layer of the water disregarding the respiration happening deeper down. A deeper z_{lim} based on the deepest z_{eup}, instead, accounts for all the respiration happening in the deeper parts when the euphotic layer is thinner. The mean difference between N determined using z_{lim} = 45, 60 and 75 m was used as a measure of the uncertainty associated with N_{eup} (± 6.3 mmol m^{-2} d^{-1}, ± 2.1 mol m^{-2}, ± 30%).

Another test was performed to assess the sensitivity of the method to the 7-day length of the averaging bins. N was recalculated binning over 1 day, 3 days, 5 days, 7 days, 9 days, 11 days, 13 days and 15 days (Table A2). The maximum change with respect to the values averaged over 7-day bins was obtained using 15-day bins, which increased mean N by 6.5%. This value was one order of magnitude smaller than the uncertainty related to changes in z_{lim} so was ignored in the error budget. Therefore, the uncertainty of ± 30% estimated from the choice of z_{lim} was used, as the uncertainty introduced by different bin lengths was considered to be negligible in comparison.

Appendix C. Supplementary material

Supplementary data to this article can be found online at https://doi.org/10.1016/j.pocean.2020.102293.

References

Alkire, M.B., D'asaro, E., Lee, C., Jane Perry, M., Gray, A., Cetinić, I., Briggs, N., Rehm, E., Kallin, E., Kaiser, J., González-Posada, A., 2012. Estimates of net community production and export using high-resolution, Lagrangian measurements of O2, NO3−, and POC through the evolution of a spring diatom bloom in the North Atlantic. Deep Sea Research Part I: Oceanographic Research Papers 64, 157–174.

Alkire, M.B., Lee, C., D'Asaro, E., Perry, M.J., Briggs, N., Cetinić, I., Gray, A., 2014. Net community production and export from Seaglider measurements in the North Atlantic after the spring bloom. J. Geophys. Res. Oceans 119, 6121–6139.

Babin, S.M., Carton, J.A., Dickey, T.D., Wiggert, J.D., 2004. Satellite evidence of hurricane-induced phytoplankton blooms in an oceanic desert. J. Geophys. Res. Oceans 109.

Barton, A.D., Finkel, Z.V., Ward, B.A., Johns, D.G., Follows, M.J., 2013. On the roles of cell size and trophic strategy in North Atlantic diatom and dinoflagellate communities. Limnol. Oceanogr. 58. https://doi.org/10.4319/lo.2013.58.1.0254.

Beckmann, A., Hense, I., 2007. Beneath the surface: Characteristics of oceanic ecosystems

under weak mixing conditions – A theoretical investigation. Prog. Oceanogr. 75, 771–796.
Behrenfeld, M.J., 2010. Abandoning Sverdrup's Critical Depth Hypothesis on phytoplankton blooms. Ecology 91, 977–989.
Bender, M., Ducklow, H.W., Kiddon, J.J.M., Martin, J., 1992. The carbon balance during the 1989 spring bloom in the North Atlantic Ocean, 47N/20W. Deep Sea Res. 39, 1707–1725.
Benson, B.B., Krause, D., 1984. The concentration and isotopic fractionation of oxygen dissolved in freshwater and seawater in equilibrium with the atmosphere1. Limnol. Oceanogr. 29 (3), 620–632.
Brody, S.R., Lozier, M.S., Dunne, J.P., 2013. A comparison of methods to determine phytoplankton bloom initiation. J. Geophys. Res. Oceans 118 (5), 2345–2357.
Broecker, W.S., Peng, T.-H., 1992. Interhemispheric transport of carbon dioxide by ocean circulation. Nature 356, 587–589.
Brunet, C., Casotti, R., Vantrepotte, V., 2008. Phytoplankton diel and vertical variability in photobiological responses at a coastal station in the Mediterranean Sea. J. Plankton Res. 30, 645–654.
Castro-Morales, K., Kaiser, J., 2012. Using dissolved oxygen concentrations to determine mixed layer depths in the Bellingshausen Sea. Ocean Sci. 8, 1–10.
Cetinić, I., Toro-Farmer, G., Ragan, M., Oberg, C., Jones, B.H., 2009. Calibration procedure for Slocum glider deployed optical instruments. Opt. Express 17, 15420–15430.
Chester, R., 2000. Marine Geochemistry, second ed. Blackwell, Malden, Mass.
Chiswell, S.M., 2011. Annual cycles and spring blooms in phytoplankton: don't abandon Sverdrup completely. Marine Ecol. Prog. Ser. 443, 39–50.
Claustre, H., Kerhervé, P., Marty, J.C., Prieur, L., 1994. Phytoplankton photoadaptation related to some frontal physical processes. J. Mar. Syst. 5 (3–5), 251–265.
Cole, H.S., Henson, S., Martin, A.P., Yool, A., 2015. Basin-wide mechanisms for spring bloom initiation: how typical is the North Atlantic? ICES J. Mar. Sci.: Journal du Conseil.
Colebrook, J.M., 1982. Continuous plankton records: seasonal variations in the distribution and abundance of plankton in the North Atlantic Ocean and the North Sea. J. Plankton Res. 4, 435–462.
Culberson, C.H., 1991. Dissolved Oxygen. WHP Operations and Methods. Unpublished manuscript, p. 15.
Damerell, G.M., Heywood, K.J., Thompson, A.F., Binetti, U., Kaiser, J., 2016. The vertical structure of upper ocean variability at the porcupine abyssal plain during 2012–2013. J. Geophys. Res. - Oceans Submitted.
Dandonneau, Y., Deschamps, P.-Y., Nicolas, J.-M., Loisel, H., Blanchot, J., Montel, Y., Thieuleux, F., Bécu, G., 2004. Seasonal and interannual variability of ocean color and composition of phytoplankton communities in the North Atlantic, equatorial Pacific and South Pacific. Deep Sea Res. Part II 51, 303–318.
De Boyer Montegut, C., Madec, G., Fischer, A.S., Lazar, A., Iudicone, D., 2004. Mixed layer depth over the global ocean: An examination of profile data and a profilebased climatology. J. Geophys. Res. 109.
del Giorgio, P.A., Cole, J.J., Cimbleris, A., 1997. Respiration rates in bacteria exceed phytoplankton production in unproductive aquatic systems. Nature 385, 148–151.
del Giorgio, P.A., Duarte, C.M., 2002. Respiration in the open ocean. Nature 420, 379–384.
Delauney, L., Compere, C., Lehaitre, M., 2010. Biofouling protection for marine environmental sensors. Ocean Sci. 6, 503–511.
Denaro, G., Valenti, D., la Cognata, A., Spagnolo, B., Bonanno, A., Basilone, G., Mazzola, S., Zgozi, S.W., Aronica, S., Brunet, C., 2013. Spatiotemporal behaviour of the deep chlorophyll maximum in Mediterranean Sea: development of a stochastic model for picophytoplankton dynamics. Ecol. Complexity 13, 21–34.
Dickson, A.G., 1996. Determination of dissolved oxygen in seawater by Winkler titration. WOCE Operations Manual. Volume 3: The Observational Programme. Volume 3. Section 3.1: WOCE Hydrographic Programme. Part 3.1.3: WHP Operations and Methods, edited by World Ocean Circulation Experiment, Woods Hole, Massachusetts, USA.
Dimier, C., Giovanni, S., Ferdinando, T., Brunet, C., 2009. Comparative ecophysiology of the xanthophyll cycle in six marine phytoplanktonic species. Protist 160, 397–411.
Duarte, C.M., Agustí, S., 1998. The CO2 balance of unproductive aquatic ecosystems. Science 281, 234–236.
Duarte, C.M., Regaudie-De-gioux, A., Arrieta, J.M., Delgado-Huertas, A., Agustí, S., 2013. The oligotrophic ocean is heterotrophic. Ann. Rev. Mar. Sci. 5, 551–569.
Ducklow, H.W., Doney, S.C., 2013. What is the metabolic state of the oligotrophic ocean? A debate. Ann. Rev. Mar. Sci. 5, 525–533.
Duteil, O., Koeve, W., Oschlies, A., Bianchi, D., Galbraith, E., Kriest, I., Matear, R., 2013. A novel estimate of ocean oxygen utilisation points to a reduced rate of respiration in the ocean interior. Biogeosciences 10, 7723–7738.
Dutkiewicz, S., Follows, M., Marshall, J., Gregg, W.W., 2001. Interannual variability of phytoplankton abundances in the North Atlantic. Deep Sea Res. Part II 48, 2323–2344.
Egge, J.K., Aksnes, D.L., 1992. Silicate as regulating nutrient in phytoplankton competition. Mar. Ecol. Prog. Ser. Oldendorf 83 (2), 281–289.
Emerson, S., Stump, C., Nicholson, D., 2008. Net biological oxygen production in the ocean: remote in situ measurements of O2 and N2 in surface waters. Global Biogeochem. Cycles 22, GB3023.
Enriquez, R.M., Taylor, J.R., 2015. Numerical simulations of the competition between wind-driven mixing and surface heating in triggering spring phytoplankton blooms. ICES J. Mar. Sci.: Journal du Conseil 72, 1926–1941.
Falkowski, P.G., Barber, R.T., Smetacek, V., 1998. Biogeochemical controls and feedbacks on ocean primary production. Science 281, 200–206.
Fennel, K., Boss, E., 2003. Subsurface maxima of phytoplankton and chlorophyll: steadystate solutions from a simple model. Limnol. Oceanogr. 48, 1521–1534.
Field, C.B., Behrenfeld, M.J., Randerson, J.T., Falkowski, P., 1998. Primary production of the biosphere: integrating terrestrial and oceanic components. Science 281, 237–240.
Findlay, H.S., Yool, A., Nodale, M., Pitchford, J.W., 2006. Modelling of autumn plankton bloom dynamics. J. Plankton Res. 28, 209–220.
Frigstad, H., Henson, S.A., Hartman, S.E., Omar, A.M., Jeansson, E., Cole, H., Pebody, C., Lampitt, R.S., 2015. Links between surface productivity and deep ocean particle flux at the Porcupine Abyssal Plain sustained observatory. Biogeosciences 12, 5885–5897.
Garcia, H.E., Gordon, L.I., 1992. Oxygen solubility in seawater: better fitting equations. Limnol. Oceanogr. 37, 1307–1312.
Gilbert, J.A., Steele, J.A., Caporaso, J.G., Steinbrück, L., Reeder, J., Temperton, B., Huse, S., McHardy, A.C., Knight, R., Joint, I., Somerfield, P., 2012. Defining seasonal marine microbial community dynamics. ISME J. 6 (2), 298.
Goericke, R., Montoya, J.P., 1998. Estimating the contribution of microalgal taxa to chlorophyll a in the field variations of pigment ratios under nutrient and light-limited growth. Mar. Ecol. Prog. Ser. 169, 97–112.
Hamme, R.C., Emerson, S., 2006. Constraining bubble dynamics and mixing with-dissolved gases: implications for productivity measurements by oxygen mass balance. J. Mar. Res. 64, 73–95.
Hansell, D.A., Carlson, C.A., Repeta, D.J., Schlitzer, R., 2009. Dissolved organic matter in the ocean: a controversy stimulates new insights. Oceanography 22, 202–211.
Hartman, S.E., Larkin, K.E., Lampitt, R.S., Lankhorst, M., Hydes, D.J., 2010. Seasonal and inter-annual biogeochemical variations in the Porcupine Abyssal Plain 2003–2005 associated with winter mixing and surface circulation. Deep Sea Res. Part II 57 (15), 1303–1312.
Henriksen, P., Riemann, B., Kaas, H., Sørensen, H.M., Sørensen, H.L., 2002. Effects of nutrient-limitation and irradiance on marine phytoplankton pigments. J Plankton Res. 24, 835–858.
Henson, S.A., Robinson, I., Allen, J.T., Waniek, J.J., 2006. Effect of meteorological conditions on interannual variability in timing and magnitude of the spring bloom in the Irminger Basin, North Atlantic. Deep Sea Res. Part I 53, 1601–1615.
Henson, S.A., Dunne, J.P., Sarmiento, J.L., 2009. Decadal variability in North Atlantic phytoplankton blooms. J. Geophys. Res. Oceans 1978–2012, 114.
Heupel, M.R., Reiss, K.L., Yeiser, B.G., Simpfendorfer, C.A., 2008. Effects of biofouling on performance of moored data logging acoustic receivers. Limnol. Oceanogr. Methods 6, 327–335.
Huisman, J., Oostveen, P.V., Weissing, F.J., 1999. Critical depth and critical turbulence: two different mechanisms for the development of phytoplankton blooms. Limnol. Oceanogr. 44, 1781–1787.
Huisman, J., Sharples, J., Stroom, J.M., Visser, P.M., Kardinaal, W.E.A., Verspagen, J.M.H., Sommeijer, B., 2004. Changes in turbulent mixing shift competition for light between phytoplankton species. Ecology 85, 2960–2970.
Hull, T., Greenwood, N., Kaiser, J., Johnson, M., 2016. Uncertainty and sensitivity in optode-based shelf-sea net community production estimates. Biogeosciences 13, 934–959.
Ito, T., Follows, M.J., Boyle, E.A., 2004. Is AOU a good measure of respiration in the oceans? Geophys. Res. Lett. 31, n/a-n/a.
Kahru, M., Brotas, V., Manzano-Sarabia, M., Mitchell, B.G., 2011. Are phytoplankton blooms occurring earlier in the Arctic? Glob. Change Biol. 17, 1733–1739.
Kaiser, J., Reuer, M.K., Barnett, B., Bender, M.L., 2005. Marine productivity estimates from continuous O2/Ar ratio measurements by membrane inlet mass spectrometry. Geophys. Res. Lett 32.
Karl, D.M., Laws, E.A., Morris, P., Williams, P.J.L., Emerson, S., 2003. Global carbon cycle (communication arising): Metabolic balance of the open sea. Nature 426, 32.
Keeling, R.F., Körtzinger, A., Gruber, N., 2010. Ocean deoxygenation in a warming world. Annu. Rev. Mar. Sci. 2, 199–229.
Kinkade, C.S., Marra, J., Dickey, T.D., Weller, R., 2001. An annual cycle of phytoplankton biomass in the Arabian Sea, 1994–1995, as determined by moored optical sensors. Deep Sea Research Part II: Topical Studies in Oceanography 48 (6–7), 1285–1301.
Klausmeier, C.A., Litchman, E., 2001. Algal games: the vertical distribution of phytoplankton in poorly mixed water columns. Limnol. Oceanogr. 46, 1998–2007.
Klausmeier, C.A., Litchman, E., Levin, S.A., 2007. A model of flexible uptake of two essential resources. J. Theor. Biol. 246, 278–289.
Körtzinger, A., Koeve, W., Kähler, P., Mintrop, L., 2001. C: N ratios in the mixed layer during the productive season in the northeast Atlantic Ocean. Deep Sea Res. Part I 48, 661–688.
Körtzinger, A., Schimanski, J., Send, U., Wallace, D., 2004. The ocean takes a deep breath. Science 306, 1337.
Körtzinger, A., Send, U., Lampitt, R.S., Hartman, S., Wallace, D.W.R., Karstensen, J., Villagarcia, M.G., Llinás, O., Degrandpre, M.D., 2008. The seasonal pCO2 cycle at 49°N/16.5°W in the Northeastern Atlantic Ocean and what it tells us about biological productivity. J. Geophys. Res. Oceans 113, C04020.
Krahmann, G., Kanzow, T., Karstensen, J., Schlundt, M. 2011. Results from a Glider Swarm Experiment near Cape Verde. http://eprints.uni-kiel.de/12248/1/EGO_2011_-_Gerd_Krahmann.pdf.
Leterme, S.C., Edwards, M., Seuront, L., Attrill, M.J., Reid, P.C., John, A.W.G., 2005. Decadal basin-scale changes in diatom, dinoflagellates, and phytoplankoton color across the North Atlantic. Limnol. Oceanogr. 50, 1244–1253. https://doi.org/10.4319/lo.2005.50.4.1244.
Letscher, R.T., Moore, J.K., 2017. Modest net autotrophy in the oligotrophic ocean. Global Biogeochemical Cycles 31 (4), 699–708.
Lévy, M., Lehahn, Y., André, J.-M., Mémery, L., Loisel, H., Heifetz, E., 2005. Production regimes in the northeast Atlantic: a study based on Sea-viewing Wide Field-of-view Sensor (SeaWiFS) chlorophyll and ocean general circulation model mixed layer depth. J. Geophys. Res. Oceans 110.
Lobe, H., 2015. October. Recent advances in biofouling protection for oceanographic instrumentation. In: OCEANS 2015-MTS/IEEE Washington. IEEE, pp. 1–4.
Longhurst, A.L., 1998. Ecological geography of the sea. San Diego: Academic Press.

Longhurst, A., Sathyendranath, S., Platt, T., Caverhill, C., 1995. An estimate of global primary production in the ocean from satellite radiometer data. J. Plankton Res. 17 (6), 1245–1271.
Manov, D.V., Chang, G.C., Dickey, T.D., 2004. Methods for reducing biofouling of moored optical sensors. J. Atmos. Oceanic Technol. 21, 958–968.
Margalef, R., 1978. Life-forms of phytoplankton as survival alternatives in an unstable environment. Oceanol. Acta 1, 493–509.
Marra J., Bidigare, R. R. & D., D. T. 1990. Nutrients and mixing, chlorophyll and phytoplankton growth. Deep Sea Res. 37, 127-143.
Martinez, E., Antoine, D., D'Ortenzio, F., de Boyer Montégut, C., 2011. Phytoplankton spring and fall blooms in the North Atlantic in the 1980s and 2000s. J. Geophys. Res. Oceans 116.
Martin-Jézéquel, V., Hildebrand, M., Brzezinski, M.A., 2000. Silicon metabolism in diatoms: implications for growth. J. Phycol. 36 (5), 821–840.
Mcquatters-Gollop, A., Raitsos, D., Edwards, M., Attrill, M.J., 2007. Spatial patterns of diatom and dinoflagellate seasonal cycles in the NE Atlantic Ocean. Mar. Ecol. Prog. Ser. 339, 301–306. https://doi.org/10.3354/meps339301.
Moline, M.A., Wendt, D., 2011. Evaluation of glider coatings against biofouling for improved flight performance. DTIC Document.
Neuer, S., Cianca, A., Helmke, P., Freudenthal, T., Davenport, R., Meggers, H., Knoll, M., Santana-Casiano, J.M., González-Davila, M., Rueda, M.-J., Llinás, O., 2007. Biogeochemistry and hydrography in the eastern subtropical North Atlantic gyre. Results from the European time-series station ESTOC. Prog. Oceanogr. 72, 1–29.
Nicholson, D., Emerson, S., Eriksen, C.C., 2008. Net community production in the deep euphotic zone of the subtropical North Pacific gyre from glider surveys. Limnol. Oceanogr. 53, 2226–2236.
Nicholson, D.P., Wilson, S.T., Doney, S.C., Karl, D.M., 2015. Quantifying subtropical North Pacific gyre mixed layer primary productivity from Seaglider observations of diel oxygen cycles. Geophys. Res. Lett. 42, 4032–4039.
Nightingale, P.D., Malin, G., Law, C.S., Watson, A.J., Liss, P.S., Liddicoat, M.I., Boutin, J., Upstill-Goddard, R.C., 2000. In situ evaluation of air-sea gas exchange parameterizations using novel conservative and volatile tracers. Global Biogeochem. Cycles 14 (1), 373–387.
Ostle, C., Johnson, M., Landschützer, P., Schuster, U., Hartman, S., Hull, T., Robinson, C., 2015. Net community production in the North Atlantic Ocean derived from Volunteer Observing Ship data. Global Biogeochem. Cycles 29, 80–95.
Pollard, R.T., 1980. Properties of near-surface inertial oscillations. J. Phys. Oceanogr. 10, 385–398.
Quay, P.D., Stutsman, J., Steinhoff, T., 2012. Primary production and carbon export rates across the subpolar N. Atlantic Ocean basin based on triple oxygen isotope and dissolved O2 and Ar gas measurements. Global Biogeochem. Cycles 26.
Regaudie-De-gioux, A., Lasternas, S., Agustí, S., Duarte, C., 2014. Comparing marine primary production estimates through different methods and development of conversion equations. Front. Mar. Sci. 1.
Rippeth, T.P., Palmer, M.R., Simpson, J.H., Fisher, N.R., Sharples, J., 2005. Thermocline mixing in summer stratified continental shelf seas. Geophys. Res. Lett. 32.
Rippeth, T.P., Wiles, P., Palmer, M.R., Sharples, J., Tweddle, J., 2009. The diapcynal nutrient flux and shear-induced diapcynal mixing in the seasonally stratified western Irish Sea. Cont. Shelf Res. 29, 1580–1587.
Rumyantseva, Anna, Henson, Stephanie, Martin, Adrian, Thompson, Andrew F., Damerell, Gillian M., Kaiser, Jan, Heywood, Karen J., 2019. Phytoplankton spring bloom initiation: The impact of atmospheric forcing and light in the temperate North Atlantic Ocean. Prog. Oceanogr. 178, 102202. https://doi.org/10.1016/j.pocean.2019.102202.
Rumyantseva, A., Lucas, N., Rippeth, T., Martin, A., Painter, S.C., Boyd, T.J., Henson, S., 2015. Ocean nutrient pathways associated with the passage of a storm. Global Biogeochem. Cycles 29, 1179–1189.
Russell, J.L., Dickson, A.G., 2003. Variability in oxygen and nutrients in South Pacific Antarctic Intermediate. Water. Global Biogeochem. Cycles 17.
Sakshaug, E., Bricaud, A., Dandonneau, Y., Falkowski, P.G., Kiefer, D.A., Legendre, L., Morel, A., Parslow, J., Takahashi, M., 1997. Parameters of photosynthesis: definitions, theory and interpretation of results. J. Plankton Res. 19 (11), 1637–1670.
Son, S., Platt, T., Bouman, H., Lee, D., Sathyendranath, S., 2006. Satellite observation of chlorophyll and nutrients increase induced by Typhoon Megi in the Japan/East Sea. Geophys. Res. Lett. 33.
Song, L., Liu, Z., Wang, F., 2015. Comparison of wind data from ERA-Interim and buoys in the Yellow and East China Seas. Chinese J. Oceanol. Limnol. 33 (1), 282–288.
Stramska, M., Stramski, D., 2005. Effects of a nonuniform vertical profile of chlorophyll concentration on remote-sensing reflectance of the ocean. Appl. Opt. 44 (9), 1735–1747.
Sverdrup, H.U., 1953. On conditions for the vernal blooming of phytoplankton. J. Conseil 18, 287–295.
Taylor, J.R., Ferrari, R., 2011. Shutdown of turbulent convection as a new criterion for the onset of spring phytoplankton blooms. Limnol. Oceanogr. 56, 2293–2307.
Tengberg, A., Hovdenes, J., Barranger, D., Brocandel, O., Diaz, R., Sarkkula, J., Huber, C., Stangelmayer, A., 2003. Optodes to measure oxygen in the aquatic environment -Dr. Anders Tengberg (Goteborg University), Jostein Hovdenes (Aanderaa Instruments A/S), Dennis Barranger, Olivier Brocandel (Nereides), Dr. Sea Technology 44 (2), 10–16.
Thompson, A.F., Lazar, A., Buckingham, C.E., Naveira Garabato, A.C., Damerell, G.M., Heywood, K.J., 2016. Open-ocean submesoscale motions: a full seasonal cycle of mixed layer instabilities from gliders. J. Phys. Oceanogr. 46, 1285–1307.
Tosteson, T.R., Zaidi, B.R., Revuelta, R., Iman, S.H., Axtmayer, R.W., De Vore, D., Ballantine, D.L., Sasscer, D.S., Morgan, T.O., Rivera, C., 1982. OTEC biofouling, corrosion, and materials study from a moored platform at Punta Tuna, Puerto Rico. II. Microbiofouling. Ocean Sci. Eng.
Ueyama, R., Monger, B.C., 2005. Wind-induced modulation of seasonal phytoplankton blooms in the North Atlantic derived from satellite observations. Limnol. Oceanogr. 50, 1820–1829.
Veldhuis, M.J.W., Kraay, G.W., 2004. Phytoplankton in the subtropical Atlantic Ocean: towards a better assessment of biomass and composition. Deep Sea Res. Part I 51, 507–530.
Whelan, A., Regan, F., 2006. Antifouling strategies for marine and riverine sensors. J. Environ. Monit. 8, 880–886.
Williams, P.J.L.B., 1998. The balance of plankton respiration and photosynthesis in the open oceans. Nature 394, 55–57.
Williams, P.J.L.B., Bowers, D.G., 1999. Regional carbon imbalances in the oceans. Science 284, 1735.
Williams, C., Sharples, J., Mahaffey, C., Rippeth, T., 2013. Wind-driven nutrient pulses to the subsurface chlorophyll maximum in seasonally stratified shelf seas. Geophys. Res. Lett. 40, 5467–5472.
Woolf, D.K., Thorpe, S.A., 1991. Bubbles and the air-sea exchange of gases in nearsaturation conditions. J. Mar. Res. 49, 435–466.
Wu, Y., Platt, T., Tang, C.C.L., Sathyendranath, S., Devred, E., Gu, S., 2008. A summer phytoplankton bloom triggered by high wind events in the Labrador Sea, July 2006. Geophys. Res. Lett. 35.
Zhai, L., Platt, T., Tang, C., Sathyendranath, S., Walne, A., 2013. The response of phytoplankton to climate variability associated with the North Atlantic Oscillation. Deep Sea Res. Part II 93, 159–168.